Developing a phenology- and pixel-based algorithm for mapping rapeseed at 10m spatial resolution using multi-source data

Jichong Han[1], Zhao Zhang[1], Yuchuan Luo[1], Juan Cao[1], Liangliang Zhang[1], Jing Zhang[1], Ziyue Li[1]

[1]State Key Laboratory of Earth Surface Processes and Resource Ecology/ MoE Key Laboratory of Environmental Change and Natural Hazards, Faculty of Geographical Science, Beijing Normal University, Beijing 100875, China

Correspondence to: Zhao Zhang (sunny_zhang@bnu.edu.cn)

Abstract. As a major oilseed crop, large-scale and high-resolution maps of rapeseed (Brassica napus L.) are critical for predicting annual production and ensuring global energy security. However, such free maps are still unavailable in large areas. We designed a new pixel- and phenology-based algorithm and produced a new data product for rapeseed planting area (2017-2019) over 33 countries at 10-m spatial resolution based on the multiple data. The product showed a good consistence (R^2=0.88) with the official statistics (Food and Agricultural Organization of the United Nations, FAO) at national level. Rapeseed maps achieved at least 0.81 F1-scores of spatial consistency when comparing with the Cropland Data Layer (CDL) of America, Annual Crop Inventory (ACI) in Canada and Crop Map of England (CROME) in England. Moreover, their F1-scores ranged 0.84-0.92 based on the independent validation samples, implying a good consistency with ground truth. Furthermore, we found that rapeseed crop rotation is ≥2 years in almost all countries. Our derived maps with high accuracy suggest the robustness of pixel- and phenology-based algorithm in identifying rapeseed over large regions with various climate and landscapes. The derived rapeseed planting areas freely downloaded can be applied to predict rapeseed production and optimize planting structure. The product is available publicly at http://dx.doi.org/10.17632/ydf3m7pd4j.3 (Han et al., 2021).

1 Introduction

Currently, fossil fuels are the main source of energy (Fang et al., 2016; Shafiee and Topal, 2009). However, overexploiting fossil fuels will exposure human increasing risks such as nonrenewable fossil fuels, greenhouse gas emission, and environmental pollution (Fang et al., 2016; Höök and Tang, 2013). Biofuel energy seems to be a promising alternative energy source and has become a key concern (Hassan and Kalam, 2013). Rapeseed is not only an important biofuel, but also edible oil, animal feed, and protein meal plant species all over the world (Firrisa et al., 2014; Malça and Freire, 2009; Sulik and Long, 2016). As a widely grown winter or spring crop, the global rapeseed production has been increasing rapidly in the past few decades. Rapeseed data products on planting intensities, their health and productivity are dependent on precise and accurate planting area maps (Zhang et al., 2019). Nonetheless, such maps are yet unavailable, a great gap for global food and energy security.

Global agricultural statistics on rapeseed in many regions come from field surveys, field sampling, and producer reports (Arata
30   et al., 2020; Fuglie, 2010). Ground-based methods are time-consuming and labor-intensive and fail in describing the detailed
spatial information of rapeseed fields (Wang et al., 2020a). Remote sensing technology plays an important role in agricultural
monitoring, providing accurate and objective spatial-temporal crop information (Dong et al., 2016; Salmon et al., 2015). In
previous literature, MODIS and Landsat were used to identify different crop types over large scales (Dong et al., 2016; Gong
et al., 2013; Salmon et al., 2015; Xiao et al., 2006; Zhang et al., 2020). With a higher spatial resolution than MODIS and
35   Landsat data, Sentinel-1/2 (S1/2) show a greater power for high-resolution crop mapping (Malenovský et al., 2012; Singha et
al., 2019).

At present, many land cover products from remote sensing have provided openly a cropland layer, e.g. the Fine Resolution
Observation and Monitoring of Global Land Cover (FROM-GLC) project (Gong et al., 2013), the GLOBCOVER land-cover
maps (Arino et al., 2008), the Global Land Cover 2000 (GLC2000) map (Bartholomé and Belward, 2005), ChinaCropPhen1km
40   (Luo et al., 2020), and Global Food Security-support data at 30 m (GFSAD30) (Phalke et al., 2020; Xiong et al., 2017).
However, cropland identified by these products either failed in distinguishing different crop types or indicated by a coarse
spatio-temporal resolution (Teluguntla et al., 2018), and also excluded rapeseed information. Till nowadays, there are few
rapeseed maps on a large-scale, especially at 10m-resolution. The 30m-resolution Cropland Data Layer (Boryan et al., 2011)
for the America and Annual Crop Inventory in Canada (Fisette et al., 2013) did classify various crops using the decision tree
45   classification method based on a large volume of training samples. However, the method is hard to apply into other developing
regions due to lack of ground training samples (Xiong et al., 2017). A new method is highly required to map large-scale annual
maps with high spatial resolution, which will widely applicable for the regions with scare ground training samples.

Five remote sensing-based methods for rapeseed mapping have been developed in recent decades: a) machine learning:
supervised classifiers such as Random Forest (RF) (Griffiths et al., 2019; Preidl et al., 2020), and unsupervised classifiers such
50   as Iterative Self-Organizing Data Analysis Technique (She et al., 2015; Tao et al., 2020); b) a classifer based on time series
data: e.g. an automatic rapeseed classification method using sentinel 2 images (Ashourloo et al., 2019); c) a threshold
segmentation based on phenology(Tian et al., 2019); d) Multi-Range Spectral Feature Fitting (MRSFF) (Pan et al., 2013); and
e) HSV transformation and Spectral Features (Wang et al., 2018). However, most methods only produce rapeseed maps for a
small area based on very limited imageries taken on the rapeseed peaking flowering dates (Ashourloo et al., 2019; She et al.,
55   2015). The peak flowering dates vary by areas and cultivars because of differences in natural conditions and cultivation habits,
especially over a large-region (d'Andrimont et al., 2020; Ashourloo et al., 2019; McNairn et al., 2018). Thus, it is still a big
challenge to automatically map rapeseed areas with a finer resolution over a large region by applying the above methods.

Fortunately, as its powerful computing performance, cloud computing technology has developed rapidly (Gorelick et al., 2017)
and made high-resolution rapeseed map possible over large areas. In the last decade powerful computing performance has
60   developed, Google Earth Engine (GEE) can provide unprecedented opportunities to process large amounts of remote sensing
data with the most advanced cloud computing and storage capabilities (Gorelick et al., 2017).

Considering the unique phenological characteristics of crops, many studies have indicated the potential ways based on phenology for crop identifying in large areas (Ashourloo et al., 2019; Dong et al., 2016; Liu et al., 2018b, 2020a; Zhang et al., 2020). The algorithm based on phenology develops classification rules through analyzing the unique characteristic of the crop,

65   which have been successfully applied to map rice (Dong et al., 2016), soybean (Zhong et al., 2014), corn (Zhong et al., 2016), and sugarcane (Wang et al., 2020a), but not yet for rapeseed. Rapeseed has unique reflectance and scattering characteristics (Ashourloo et al., 2019; McNairn et al., 2018; Sulik and Long, 2015, 2016), and undergoes three canopy morphologies (Ashourloo et al., 2019; Rondanini et al., 2014), including leaves, yellow petals, and pods/branches. Each canopy shape strongly influences how solar radiation intercepts (Sulik and Long, 2016). Compared with other crops, rapeseed is more easily

70   to be identified, of which the yellow flowers significantly increase the reflectance of red and green bands (Pan et al., 2013; Sulik and Long, 2015). Additionally, when rapeseed grows, the backscatter signal increases because the rough canopy structure formed by the intertwined pods. (McNairn et al., 2018; Mercier et al., 2020; Tian et al., 2019; Veloso et al., 2017). Thus we are sure the specific featrues of reflectance values and scattering coefficients of rapeseed on S1/2 data will provide enough information for automatic rapeseed mapping over larger areas and with a finer resolution.

75   Thus, we integrated multi-source data to: 1) develop new method for identifying rapeseed ; 2) apply the new method to generate rapeseed maps with a spatial resolution of 10m in three years (2017-2019) across the main planting areas of 33 countries; 3) analyze the geographic characteristics of rapeseed planting and crop rotation. The proposed algorithm and its derived products may benefit decision-makers, scientists and local farmers to ensure food and ennerge security.

2 Materials

80   ### 2.1 Study area

This work identified rapeseed planting areas for 33 countries in three continents (North America, South America, and Europe) as they are the main rapeseed producers in the world (Fig. 1). The planting areas and production of rapeseed are large in Canada and the European Union (EU) (Carré and Pouzet, 2014; van Duren et al., 2015; Rondanini et al., 2012). According to the report by Statistics Canada, from 2000 to 2019, the rapeseed area in Canada increased by 1.7 times, and the production increased by

85   2.7 times(https://www.canolacouncil.org/). Rapeseed is grown in most European countries. The EU's rapeseed production in 2017 was approximately 1.92 times that of 2000 (d'Andrimont et al., 2020). Europe produces a large amount of biodiesel for the world every year. In 2008, 79% of the biodiesel feedstock crops in Europe were rapeseed (van Duren et al., 2015). Also, the Republic of Chile is the main rapeseed producer in South America and the country with a high yield of rapeseed in 2018 (38877 kg/ha). Rapeseed agriculture in these countries is important in food and energy security (Carré and Pouzet, 2014). The

90   climates in these three continents are different because of factors such as latitude and topography. Europe includes three climatic types: subtropics, boreal, and temperate (Fig. S1b) (Peel et al., 2007). The climate in the rapeseed growing areas in Canada and northern America is temperate and boreal (Fig. S1a). The Republic of Chile is the main subtropics climate (Fig.

S1c). Rapeseed planting seasons are different because of differences in natural conditions (such as climate and temperature) in different countries (Singha et al., 2019; Wang et al., 2018), which brings great challenges to map rapeseed.
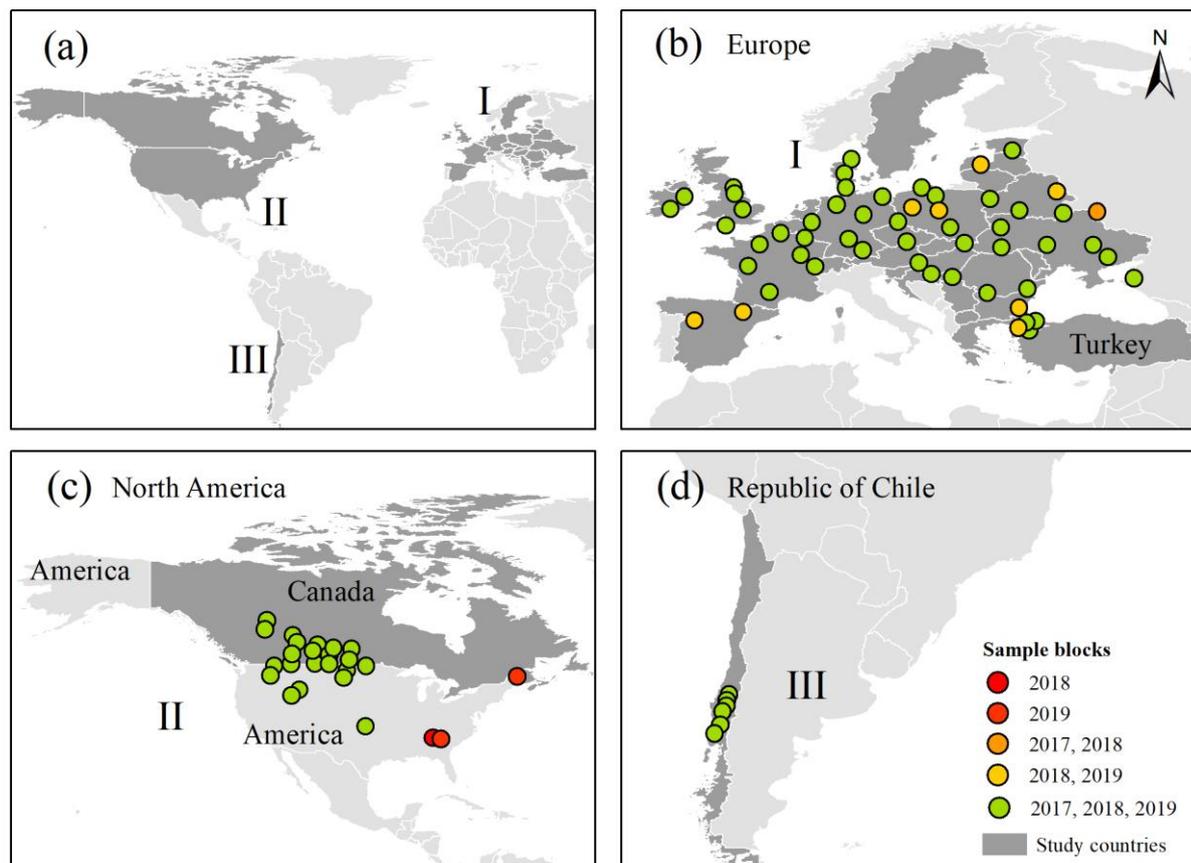
95

Figure 1. The locations of 33 countries and the sample blocks for phenological monitoring with a radius of 10km.

2.2 Data

2.2.1 Remote sensing data

We collected the Sentinel-2 (S2) and Sentinel-1 (S1) imagery (Table 1). The S1/2 satellites are launched by the European
100 Space Agency (ESA) (Drusch et al., 2012; Torres et al., 2012). The highest spatial resolution of S2 images is 10m. We used red (b4), green (b3), and blue (b2) spectral bands with 10 m spatial resolution Top-Of-Atmosphere (TOA) reflectance observations. The S2 TOA product includes the Quality Assessment (QA) band, which was used to remove most of the bad-quality images (e.g. clouds information) in this study. However, it is difficult to remove all clouds due to the quality of the QA band (Wang et al., 2020a; Zhu et al., 2015). The S1 includes four modes: Stripmap (SM), Interferometric Wide Swath (IW), 105 Extra Wide Swath (EW), and Wave (WV) (Torres et al., 2012). We used the IW mode, which provides dual-band cross-

polarization (VV) and vertical transmit/horizontal receive (VH) with a 12 day or 6-day repeat cycle and 10m space resolution (Torres et al., 2012). The S 1/2 images were obtained on GEE. Also, we used QA bands to remove most of the bad-quality images on GEE (Sample code can be found at https://code.earthengine.google.com/?scriptPath=Examples%3ADatasets%2FCOPERNICUS_S2). See Table 1 for more

110   details

2.2.2 Digital elevation model

We used a spatial resolution of one arc-second (approximately 30m) elevation data from the Space Shuttle Radar Terrain Mission (Table 1) (Farr et al., 2007). Then we calculated the spatial distribution of slop on GEE (Sample code can be found at https://code.earthengine.google.com/?scriptPath=Examples%3ADatasets%2FUSGS_SRTMGL1_003) (Fig. S1d-f). Later, we

115   extracted areas with a slope less than 10° to mask hilly terrain where rapeseed is unlikely to be planted (Jarasiunas, 2016).

2.2.3 Cropland and agricultural statistics data

In this study, cropland data from the GFSAD30 were used to identify major farming areas in different countries (Phalke et al., 2020; Xiong et al., 2017). The existing crop data products containing rapeseed information include: 1) the 30-m Annual Crop Inventory (ACI) in Canada (Fisette et al., 2013). 2) the 30-m Cropland Data Layer (CDL) was generated in America (Boryan

120   et al., 2011). CDL and ACI layers are downloaded on GEE. 3) the Crop Map of England (CROME) was generated in America in England. These three crop layer products are generated based on satellite images and a large number of training sample collections. In this study, rapeseed maps in ACI, CDL and CROME were used for accuracy verification at the pixel level. The FAO releases annual statistics on the area for major crops in different countries or regions. We selected the statistics from FAO for accuracy verification. Please see Table 1 for more details

125   **2.2.4 Crop calendars**

We used two crop phenological data sets to assist in extracting rapeseed phenological parameters: (1) crop calendars in different countries (https://ipad.fas.usda.gov/ogamaps/cropcalendar.aspx). The crop calendars come from the United States Department of Agriculture (USDA) which only record the planting and harvest time of rapeseed in some countries (Table S1). (2) field records of the crop phenology in Germany. In-situ observations come crop phenological records shared by the

130   Deutsche Wetterdienst (DWD) in Germany (Kaspar et al., 2015). The DWD provides field observations of crop phenological periods following the Biologische Bundesanstalt, Bundessortenamt, and Chemical (BBCH) scale throughout Germany (Table 1). DWD records the start date and the end date of rapeseed flowering (d'Andrimont et al., 2020; Kaspar et al., 2015). Note that both crop calendars and DWD do not contain information on the peak flowering dates of rapeseed. We used all stations that fully recorded the start and end of the flowering period from 2017 to 2019. Finally, 281, 269, and 253 stations available

135   in 2017, 2018, and 2019, respectively. (the spatial distribution of the DWD rapeseed stations can be found in Fig. S2.

Table 1 Detailed information about the data collected in this work.

Data	Time	Resolution	Institution	Version	Data access	Date of recent access	Descriptions
Sentinel-1 SAR GRD	2017-2019	10m	European Space Agency (ESA)	-	https://developers.google.com/earth-engine/datasets/catalog/COPERNICUS_S1_GRD	2020/11/15	Extracting the backscatter coefficient characteristics of rapeseed
Sentinel-2 MSI	2017-2019	10m	ESA	Level-1C	https://developers.google.com/earth-engine/datasets/catalog/COPERNICUS_S2	2020/11/15	Calculating the spectral indices after removing the cloud
Global Food Security-Support Analysis Data at 30 m (GFSAD30)	2015	30m	United States Geological Survey (USGS), NASA., et al.	V001	https://search.earthdata.nasa.gov/search?q=GFSAD30	2020/11/5	Identifying crop growing areas
The Shuttle Radar Topography Mission (SRTM)	-	30m	NASA Jet Propulsion Laboratory (JPL)	V3	https://developers.google.com/earth-engine/datasets/catalog/USGS_SRTMGL1_003	2020/10/1	Calculating slope map
Cropland Data Layer (CDL)	2017, 2019	30m	United States Department of Agriculture (USDA)	-	https://developers.google.com/earth-engine/datasets/catalog/USDA_NASS_CDL	2020/12/1	Accuracy verification of rapeseed map at pixel scale
Annual Crop Inventory (ACI)	2017, 2018	30m	Agriculture and Agri-Food Canada (AAFC)	-	https://developers.google.com/earth-engine/datasets/catalog/AAFC_ACI	2020/12/1	Accuracy verification of rapeseed map at pixel scale
Crop Map of England (CROME)	2018	hexagon cells	Rural Payments Agency (RPA)	V.09	https://data.gov.uk/dataset/fb19d34f-59e6-48e7-820a-fe5fda3019e5/crop-map-of-eneland-crome-2018	2021/1/15	Accuracy verification of rapeseed map at pixel scale
Phenological database of Germany	2017-2019	-	Deutsche Wetterdienst (DWD)	-	https://www.dwd.de/DE/leistungen/cdc/climate-data-center.html?nn=575620&lsbId=646252	2020/10/1	Identifying the phenological characteristics of rapeseed
Agricultural statistics data	2017-2019	-	Food and Agriculture Organization (FAO)	-	http://www.fao.org/faostat/en/#data/QC	2020/12/1	Verifying the accuracy of rapeseed map at national scale
Crop Calendars	-	-	United States Department of Agriculture (USDA)	-	https://ipad.fas.usda.gov/ogamaps/cropcalendar.aspx	2020/10/1	Auxiliary reference data for identifying the flowering period of rapeseed

2.3 Methods

2.3.1 Optical and SAR characteristics during the growing period of rapeseed

We selected available rapeseed parcels and in-situ observations of DWD from different climate regions and years to analyze the optical (reflectance and vegetation index) and SAR (VV, VH) characteristics of rapeseed along time. For example, Fig. 2

140   shows the time series of one rapeseed parcel around the DWD station with an id equal to 13126 in 2018. The rapeseed parcel shows unique visual characteristics during the flowering period (Fig. S3). The flower is becoming yellow when rapeseed is approaching peak flowering (Pan et al., 2013; Tao et al., 2020; Wang et al., 2018). Rapeseed is yellow-green on the true color images of S2 and Google Earth during the flowering period (Fig. S4). The reflectance of green band and red band separately increased from 0.09 and 0.06 (2018/4/17, before flowering) to 0.16 and 0.14 (2018/5/7, peak flowering), and decreased after

145   flowering (Fig. 2a). The reflectance of the blue band is lower than red and green bands during flowering. The reflectance of the red band increased again and higher than the green band during the rapeseed harvest period. This is similar to previous research results (Ashourloo et al., 2019; Sulik and Long, 2015). The Normalized Difference Yellow Index (NDYI, Eq.1) can capture the increasing yellowness in the time-series (d'Andrimont et al., 2020; Sulik and Long, 2016). Also, the NDYI increased from -0.03 on April 17 to 0.21 on May 7 (Fig. 2b). NDYI reaches a peak during the flowering time of rapeseed. This

150   unique spectral feature of rapeseed in the flowering period is caused by the yellow petals.

$$NDYI = \frac{green - blue}{green + blue} \tag{1}$$

where *green* is the TOA reflectance of the green band (b3) of the S2 imagery, *blue* is the blue band (b2) reflectance.

S1 backscattering changes with the growth of rapeseed. We used the VV and VH time series smoothed by the Savitzky–Golay (SG) filter (window size 3) (Chen et al., 2004) as input to identify the phenological parameters of rapeseed parcels. We ran the

155   SG filter algorithm on Matlab 2020a. The results show that there are local minimums in both the VV (-11.20, May 8) and VH (-15.60, May 5) time series during rapeseed flowering (Fig. 2c-d). Furthermore, VH reaches the maximum (-9.64, June 1) during the pod period (Fig. 2d). Unlike other crops, rapeseed has two distinct green up phases: the flowering period and the pod period (Ashourloo et al., 2019; Bargiel, 2017; Mercier et al., 2020; Veloso et al., 2017). The petals of rapeseed decrease the scattering of VV and VH, while the pods increase the scattering intensity of VH (d'Andrimont et al., 2020; Bargiel, 2017;

160   McNairn et al., 2009; Mercier et al., 2020). The NDYI and backscattering (VV, VH) time series of rapeseed in different climate regions (Fig. S4) also show the same characteristics. Hence, we used the features in both Optical and SAR to identify the rapeseed flowering and pod period in this study. Due to the difference in the revisit periods of S1/2 satellites, rapeseed peak flowering dates are defined as the median dates extracted by optical and SAR indicators.

 (figure panels a–e)
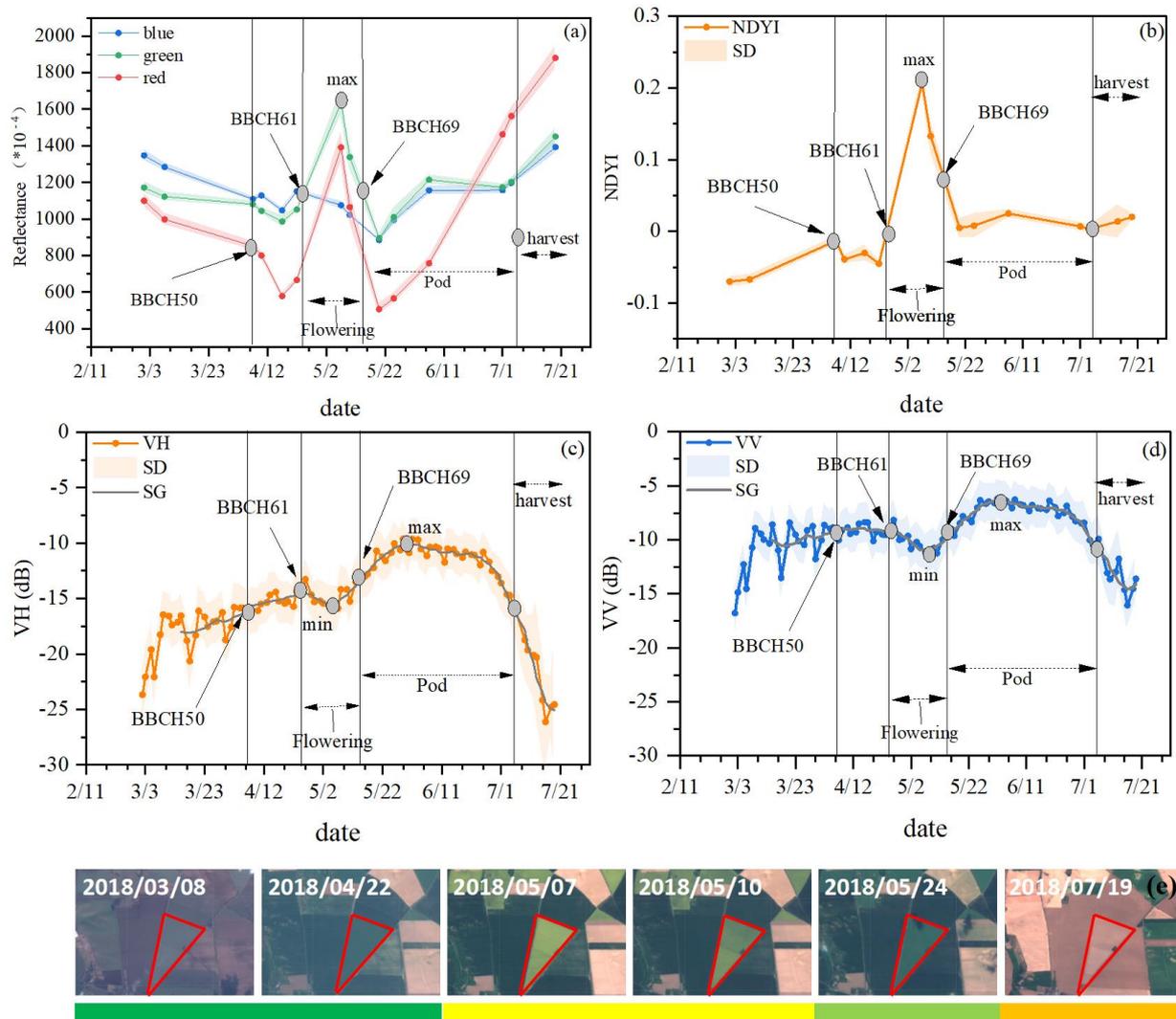
165 Figure 2. The time-series profiles of four features of the rapeseed pixels around one DWD station (id = 13126, Longitude: 11.333268424°, Latitude: 52.200000463°) in Germany in 2018. (a) the mean reflectance values (red, green, and blue); (b) mean NDYI; (c) mean VH; and (d) mean VV; the filled color areas for standard deviation; BBCH for the in-situ observations of rapeseed phenology, with BBCH61, BBCH69, and BBCH50 for the flowering, falling, sprouting, respectively. (e) The rapeseed parcel around the DWD station is shown by red boundaries (image source: Copernicus Sentinel-2 data 2018).

170 **2.3.2 Sample blocks collected for phenological monitoring**

As a pre-requisite to map rapeseed at a large-scale, the phenology of rapeseed in different countries needs to be identified and delineated (Dong et al., 2016; Zhang et al., 2020). However, not enough observation records of rapeseed phenology are available on a large scale. Referring to the DWD method of observing phenology (Kaspar et al., 2015), we created a radius of

10km sample block over rapeseed producing areas of different countries and randomly sampled 10 rapeseed parcels uniformly
175   for each block (Fig. S5). The rapeseed plots were identified by phenological characteristics obtained from visual-interpretation
and   reference data: (1) high-resolution images available in S2 and Google Earth. It should be noted that the Google Earth
images during rapeseed flowering were used to assist the visual interpretation of rapeseed parcels. (2) Spectral reflectance (red
band and green band) and spectral index (NDYI) and scattering coefficient profiles (VV and VH) from S1/2 time series. The
rapeseed parcels without high-quality available time-series imagery because of data quality issues such as clouds were omitted.
180   Finally, 75 sample blocks, 84 sample blocks, 84 sample blocks in 2017, 2018, 2019 were uniformly and randomly collected.
The sample blocks are shown in Fig. 1. We extracted the growth phenology information of rapeseed by calculating the average
of the pixels of all rapeseed parcels in each block in different regions.

2.3.3 Flowering and pod phase detection in different countries

The phenology of rapeseed is different among regions. To find out the flowering dates of rapeseed in different countries, we
185   evaluated each phenological sample block from 2017 to 2019. First, we calculated the time-series average value of S1/2 of all
sample rapeseed parcels pixels during the rapeseed growth period for each block in conjunction with the crop calendar. VV
and VH time series for each sample rapeseed parcels were smoothed using the SG filter. Second, these S1/2 peak flowering
dates and pod dates were derived for all sample blocks based on the method in Section 2.3.1. We found the peak flowering
dates of rapeseed have an explicit latitude gradient, especially in Europe (Fig. S6). Also, we found the signal with the maximum
190   of VH is within 45 days after the peak date of flowering (Fig. S7). Then we calculated the difference in the peak flowering
date of each sample block in different years. The results showed that the error were within 10 days of advance or delay (Fig.
3d). Therefore, it is reasonable to use the same time for rapeseed identification in different years in the same area in this study.
Previous studies and field observation records show that the flowering period of rapeseed is about 30 days (d'Andrimont et al.,
2020; Chen et al., 2019; Kaspar et al., 2015; She et al., 2015). Therefore, we divide each month into two-time periods (the
195   15th is the dividing line). Two consecutive half-months are defined as suitable classified flowering periods. Finally, we
designated the flowering period for each sample block based on the peak flowering dates (Fig. 3a-c).
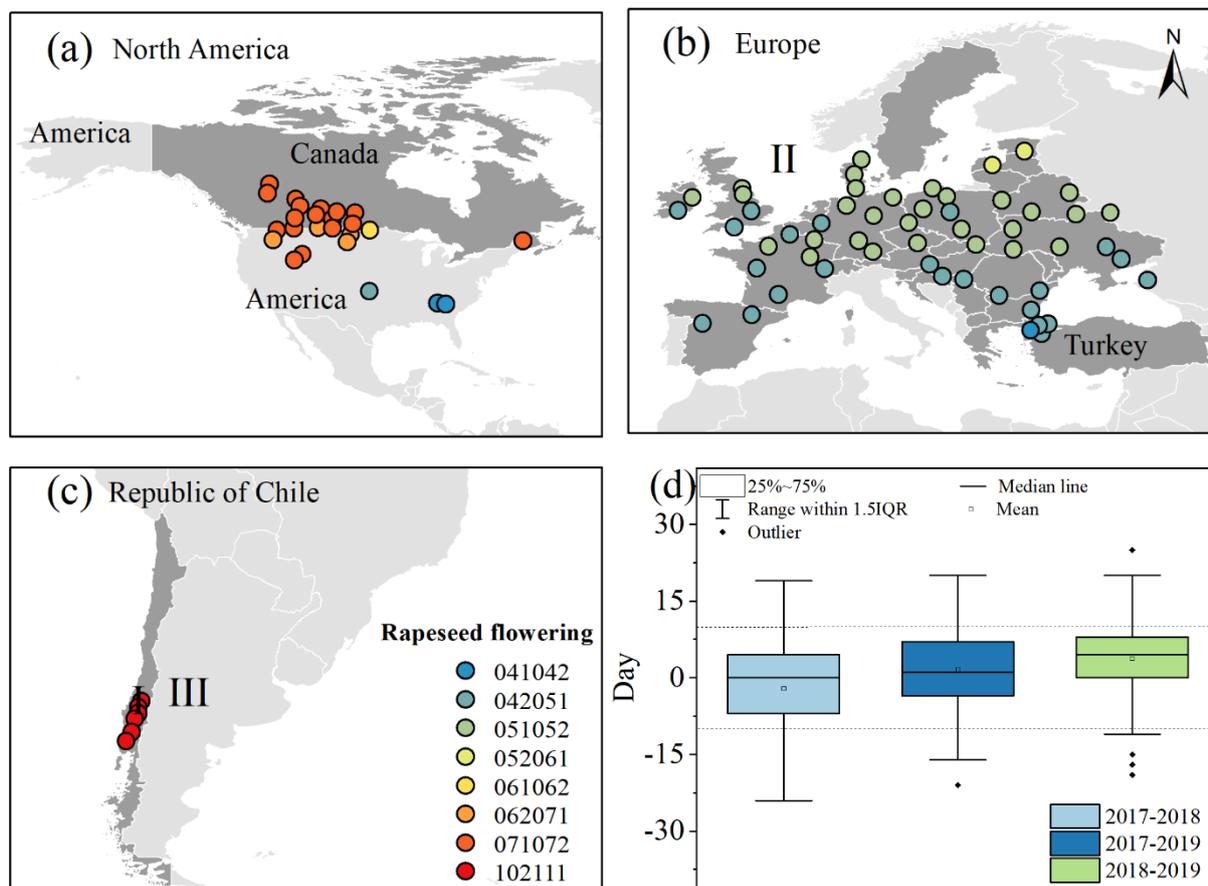
Figure 3. (a-c) The spatial distribution of rapeseed flowering periods for sample blocks (the number with six bits in Fig.3-c means: the 1st, 2nd, 4th, and 5th digits represent the month; 3rd and 6th digits represent the time of each month, where 1 and 2 represent the first half and second half of the month respectively). (d) The boxplot showing the peak flowering date of each sample block in three years.

2.3.4 Developing phenology- and pixel-based algorithm for mapping rapeseed

The temporal profile analysis at rapeseed fields in this study and many previous studies indicated that the spectrum at flowering stage and the scattering signal at pod stage are the key features to identify rapeseed (Ashourloo et al., 2019; Bargiel, 2017; Han et al., 2020; Mercier et al., 2020; Sulik and Long, 2015; Veloso et al., 2017). Previous studies have found the high reflectance values of green band and red band at the flowering stage are the main spectral factors to distinguish other crops (Ashourloo et al., 2019). We developed phenology- and pixel-based rapeseed mapping algorithm for rapeseed mapping using four features: including 1) spectral bands (red and green), 2) spectral indices (NDYI), 3) polarization bands (VH), and 4) terrain (slope). And four steps were orderly conducted for mapping annual planting areas (Fig. 5).

210 Step 1: determining the threshold of the feature indicators. Thresholds of indicators are the key parameters to determine the area accurancy identified. We analyzed the histograms of the random samples selected from different countries as the previous studies (Zou et al., 2018) suggested. We found consistently the normal distributions of green, blue, and NDYI (Fig. S9) for all samples during the flowering stage from different regions. 98% of the rapeseed pixels show red > 0.07, green > 0.11, and NDYI > 0.05.

215 However, we found some pixels with a higher NDYI, while in fact they are polluted by the cloud with a "rainbow" appearance, would be misclassified into rapeseed. Such misclassifications caused by some bad-quality observations from the S2 image cann't be removed due to the limited quality of the QA band and simple cloud score algorithm (Wang et al., 2020c; Zhu et al., 2015). The "rainbow" of the cloud is come from the push-broom design of S2 (Fig. 4a) and spectral misregistration (For more details, please refer to ESA, 2015a, and ESA, 2015b). Based on the principle of the relative displacement of each spectral

220 channel sensor in the S2 push-broom design (Frantz et al., 2018; Liu et al., 2020b; Zhao et al., 2018), we developed a new spectral index (NRGBI) to reduce the influence of "rainbow" (Eq.2). The scatter plot of NDYI and NRGBI of rapeseed field samples and "rainbow" around cloud samples (visual interpretation) show that the NRGBI (threshold is -0.05) can effectively distinguish rapeseed from the "rainbow" (Fig. 4h).

$$NRGBI = \frac{red-blue}{red+blue} - \frac{green-blue}{green+blue} \tag{2}$$

225 where *red*, *green*, and *blue* are the TOA reflectance values of the red band (b4), green band (b3), and blue band (b2) of the S2 imagery, respectively. The sample GEE code for NRGBI index calculation can be found at https://code.earthengine.google.com/a39fc699a276d018778d59c5b085d960. In addition, NRGBI can be calculated based on Eq.2 in other GIS software (e.g. QGIS and ArcGIS) of the local computer.
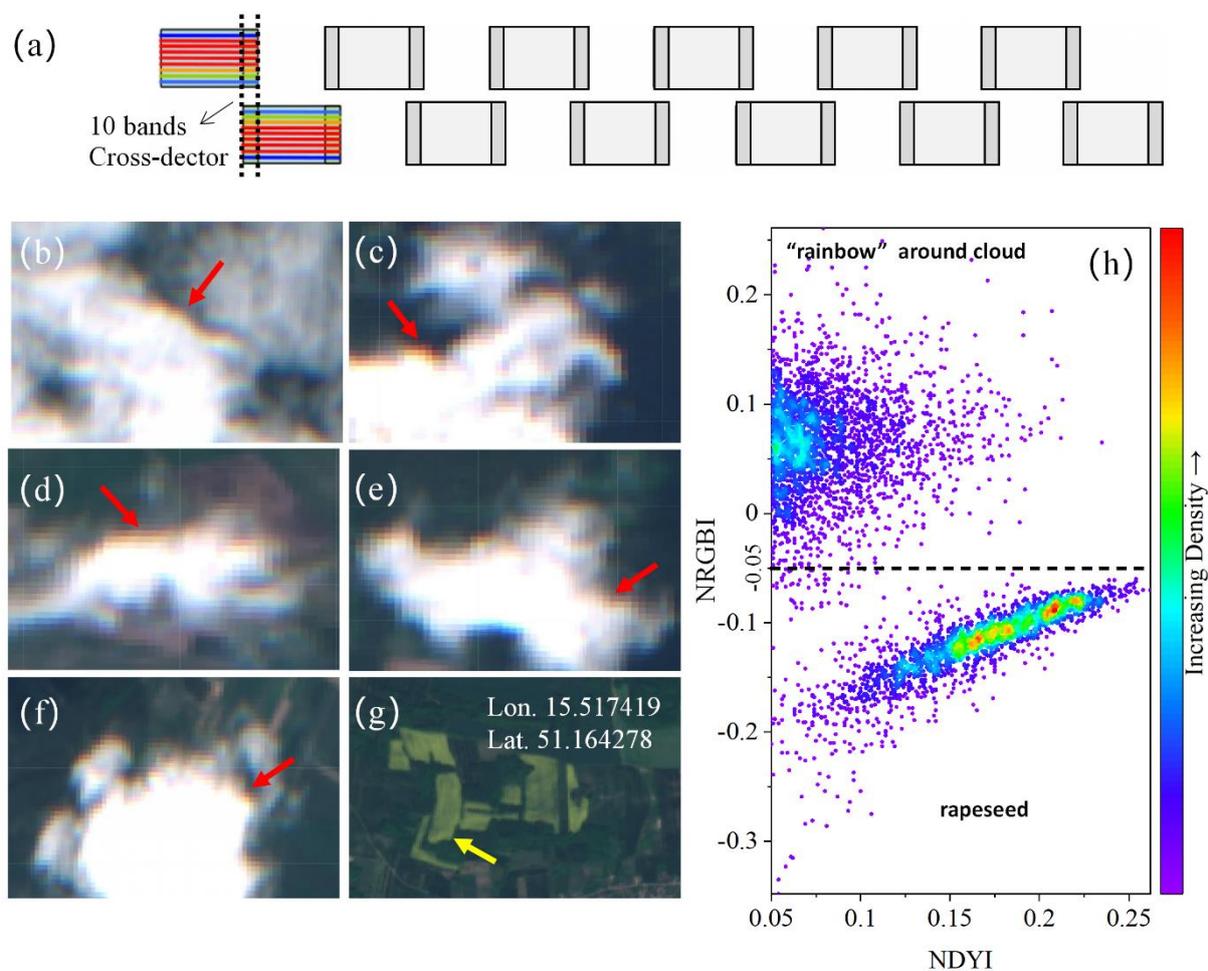
Figure 4. Causes, examples, and solutions for the "rainbow" cloud effect. a) Staggered detector configuration of S2 (ESA, 2015a); (b-f) examples of spectral misregistration effects and performance of cloud masking methods (each image was masked by quality assurance band (QA60)) for Sentinel-2 TOA image, with the red arrows indicating the cloud "rainbow" appearance at high altitude in the S2 image (image source: Copernicus Sentinel-2 data); (g) Sentinel-2 TOA image of rapeseed at the flowering stage, with the yellow arrow for the rapeseed fields; (h) scatter plots of NDYI and NRGBI of rapeseed field samples and "rainbow" around clouds samples from the S2 images, with the color density for the number of pixels.

Step 2: identifying all rapeseed pixels from different images during the flowering period and aggregating them into annual rapessed planting areas (Fig. 5). Because the peak flowering dates and the number of available images of rapeseed fields in a region are different (Fig. S10), rapeseed classifications based on single image could fail in capturing rapeseed flowering dynamics (Ashourloo et al., 2019). To avoid the misclassification from bad-quality observations during rapeseed flowering stage, the aggregate approach from all the available S2 images during the flowering period was used. Hence, a larger number of images will result in better performance (Fig. S10).

Step 3: combining optical with SAR images to ensure the accuracy of the rapeseed maps. The high VH values during the rapeseed pod stage is another distinct feature that distinguishes it from other crops (Mercier et al., 2020; Tian et al., 2019; Van Tricht et al., 2018; Veloso et al., 2017). Considering the variability of flowering in different fields and the duration of pod

245 stage (Section 2.3.2), we calculated the maximum VH during the period between the second half of the flowering stage and 30 days after it (~45 days). Within 45 days, at least three S1 satellite images are available in the study areas. Also, the areas with a slope >10° (where rapeseed is unlikely to be planted) were removed (Jarasiunas, 2016). All pixels that meet the requirements are defined as rapeseed.

Step 4: removing the "salt and pepper" noise according to the connected domain threshold of the pixels and filling the gaps

250 inside the parcels (Hirayama et al., 2019). The thresholds of different indicators in different regions can be found in Table S3.
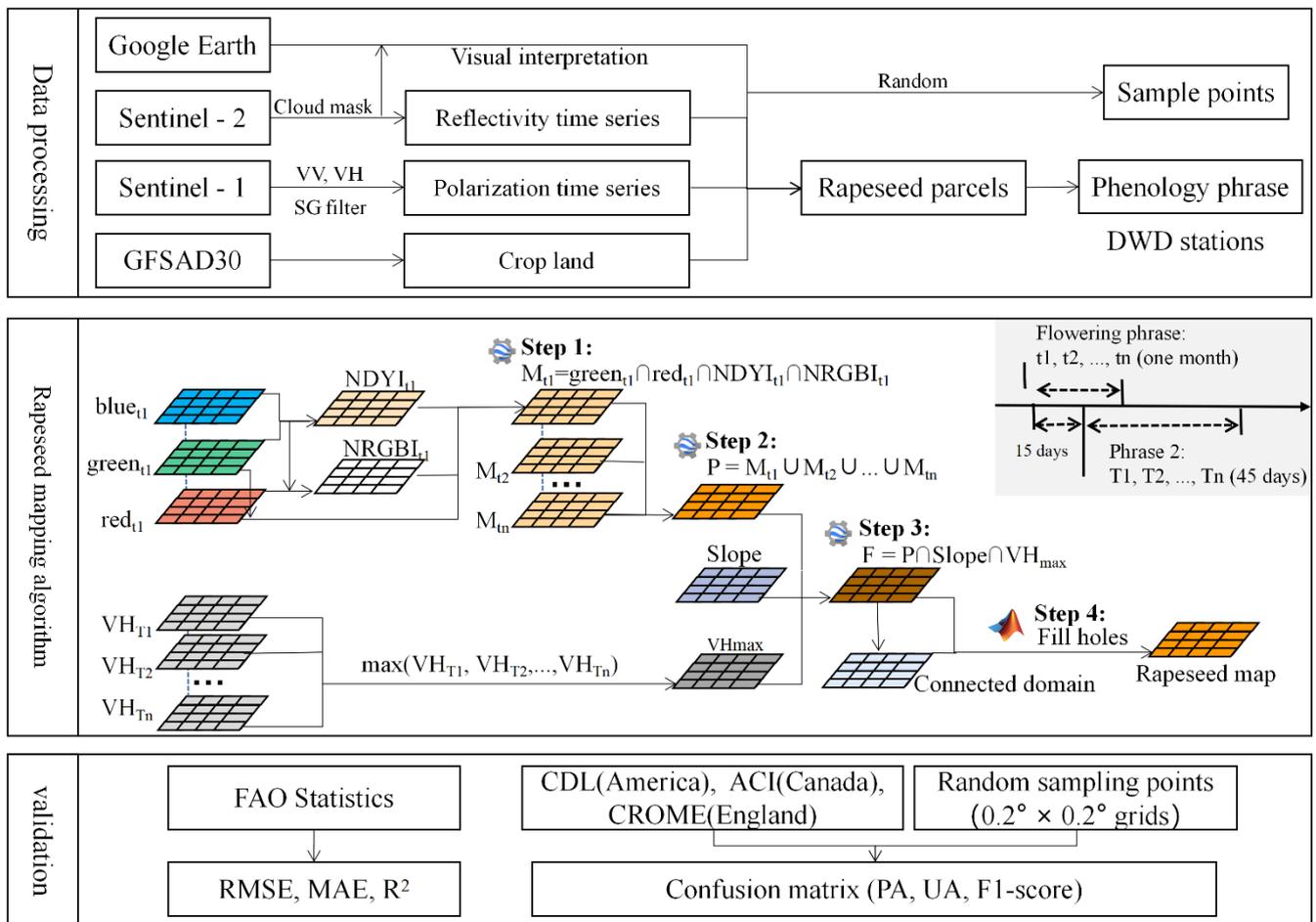
Figure 5. The workflow for mapping rapeseed areas using the new phenology- and pixel-based algorithm. Global Food Security-Support Analysis Data at 30m (GFSAD30); normalized difference yellowness index (NDYI); The new spectral index

255 (NRGBI), Deutsche Wetterdienst (DWD), Food and Agriculture Organization of the United Nations (FAO), Root Mean Square

Error (RMSE), Mean Absolute Error (MAE), R-squared (R^2), Cropland Data Layer (CDL), Annual Crop Inventory (ACI), Crop Map of England (CROME), User Accuracies (UA), Producer Accuracies (PA), and F1-score (F1).

2.4 Accuracy assessment

Total three ways were appled to assess the accuracy of rapeseed map acquired by our new phenology- and pixel-based
260 algorithm. First, we compared the rapeseed areas retrieved by the new method with FAO statistics. Our rapeseed data is a binary (0 or 1) map with a spatial resolution of 10m, equivalently as each pixel = 100 m^2. We then can calculate the total area of rapeseed map in each country and compare them with the national rapeseed statistics. The RMSE (Eq.3), and the MAE (Eq.4), and the coefficient of determination (R^2, Eq.5) are used to verify the accuracy of rapeseed mapping.

$$RMSE = \sqrt{\sum_{i=1}^{n} \frac{(y_i - f_i)^2}{n}} \tag{3}$$

265 $$MAE = \frac{1}{n}\sum_{i=1}^{n}|y_i - f_i| \tag{4}$$

$$R^2 = \frac{(\sum_{i=1}^{n}(y_i - \overline{y_i})(f_i - \overline{f_i}))^2}{\sum_{i=1}^{n}(y_i - \overline{y_i})^2 \sum_{i=1}^{n}(f_i - \overline{f_i})^2} \tag{5}$$

where n is the total number of countries. y_i is the mapped rapeseed planting areas, $\overline{y_i}$ is the corresponding mean value, f_i is the records rapeseed planting areas from FAO, $\overline{f_i}$ is the corresponding mean value.

Also, we compared the rapeseed maps with two open access datasets that include rapeseed layers (ACI, CDL and CROME) in
270 Canada, America and England on the pixel scale. We used them as the reference data for 2018, 2019 (Boryan et al., 2011; Fisette et al., 2013). To unify the spatial resolution of the rapeseed maps, CDL, ACI and CROME were resampled to 10m resolution for comparison. UA (Eq.6), PA (Eq.7), and F1 (Eq.8) were calculated based on confusion matrices (Table S2) to measure the classification accuracy.

Thirdly, we also selected randomly verification samples based on the previous studies (Pekel et al., 2016; Wang et al., 2020b)
275 to validate the rapeseed map. A grid (0.2 latitude by 0.2 longitude) was generated within the rapeseed map in 2018 acquired by our pixel- and phenology-based method. Two points (rapeseed and non-rapeseed) was generated randomly in each grid by interpreting visually images available in the S2 and Google Earth, together with spectral reflectance, spectral index and scattering coefficient profiles from S-1/2 time series. The confusion matrices were similarly used to assess the accurancy according to Eqs 6~8.

280 $$UA = \frac{x_{ij}}{x_j} \tag{6}$$

$$PA = \frac{x_{ij}}{x_i} \tag{7}$$

$$F1 = 2 \times \frac{UA \times PA}{UA + PA} \tag{8}$$

Where x_{ij} is the value of the i-th row and j-th column; x_i is the sum of the i-th row; x_j is the sum of the j-th column. Although the statistical data and existing products are not completely same as the real areas and locations of rapeseed planted on the
285 ground, these datasets do benefit to validate the accurancy of rapeseed maps at different scales (national and pixels).

3 Results

3.1 Accuracy assessment

We compared the derived rapeseed areas with those from the FAO statistics. The total planting areas of rapeseed are well consistent with the agricultural statistics at the national level, with RMSE of 1459.64 km^2, MAE of 785.25 km^2, amd R^2 of

290   0.88 (Fig. 6). We found the derived areas in 2017 and 2019 are larger than those in 2018, especially for the countries with the relative smaller rapeseed areas (e.g. many European countries indicated by the small plot located in the bottom right and below of Fig. 6. The more availability of S2 images together with better quality in 2018 could contribute the larger rapeseed areas derived by the new method (Liu et al., 2020a).
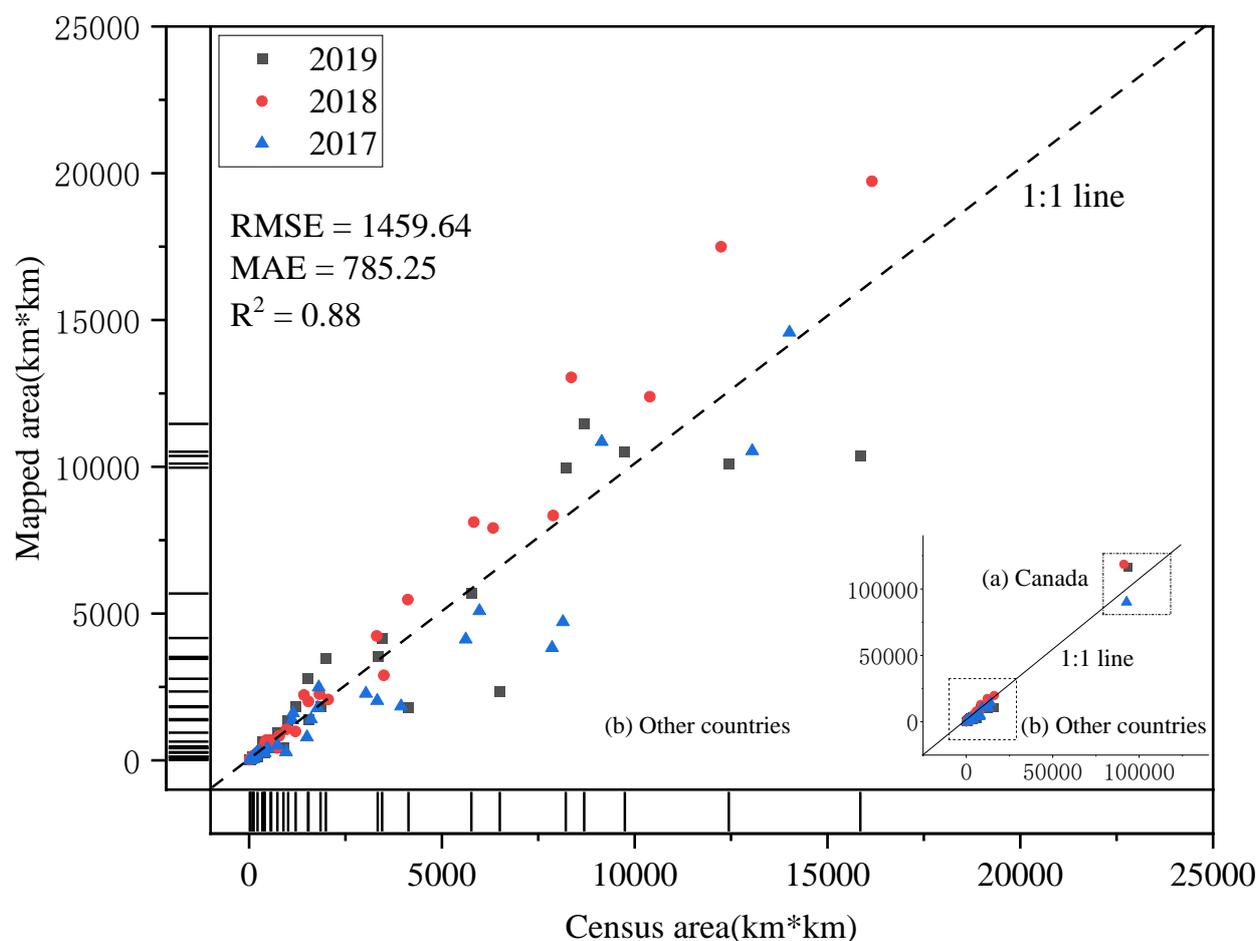
295   Figure 6. Comparison of rapeseed areas with the FAO statistics at the national level.

The comparsion of our rapeseed maps with those of America CDL in 2018, 2019, Canada ACI and England CROME in 2018 was consistently indicated by a higher accurancy according to the confusion matrices (Table 2). The UA, PA, and F1 varied

by countries, with PA of 0.71–0.80, UA of 0.93–0.96, and F1 of 0.81–0.86. The rapeseed areas retrieved by us accounted for

around 71% rapessed areas from 2018 CDL, 71% from 2018 ACI, and 80% from 2018 CROME, and 79% from 2019 CDL.

300 Table 2 The comparison of rapeseed (pixels) in Canada, America and England from different data sources in 2018, 2019, with

rows from reference classification, while columns from our derived map

		Non-rapeseed	Rapeseed	Total	PA	UA	F1
ACI 2018	Non-rapeseed		434,530,41				
	Rapeseed	469,895,705	114,144,421,6	161,133,992,1	0.71	0.96	0.82
	Total		118,489,725,7				
CDL 2018	Non-rapeseed		551,173,7				
	Rapeseed	321,272,80	778,389,57	109,966,237	0.71	0.93	0.81
	Total		833,506,94				
CDL 2019	Non-rapeseed		619,139,3				
	Rapeseed	251,284,08	935,079,60	118,636,368	0.79	0.94	0.86
	Total		996,993,53				
CROME 2018	Non-rapeseed		448,424,3				
	Rapeseed	180,611,43	712,890,46	893,501,89	0.80	0.94	0.86
	Total		757,732,89				

The confusion matrices (Table S4) based on random sampling points show that the accuracy of the rapeseed maps varies in

different regions. We found Europe shows the highest accuracy (F1 0.91), followed by Chile (F1 0.9), and the lower F1 (0.84)

indicated by North America. Such disparity in accuracy might be ascribed to the different availability of high-quality images

305 in the studied areas. Nevertheless, all rapeseed maps derived by our method show a reasonable accuracy across such a larger

region.

3.2 More details of rapeseed maps derived by the new method

To show more details of rapeseed maps derived by our method, we captured some images in some areas of each country. The

rapeseed maps show good spatial consistency with the actual rapeseed planted on the ground (Fig. 7). From the area densely

310 planted by rapeseed in Canada (Fig. 9-a) to relatively sparse planting ones such as in Chile (Fig. 9-b) and European countries

(e.g. Fig. 9-c,d) (Lowder et al., 2016), from regular rectangles (e.g. Fig. 9-a, h) to irregular parcels (Fig. 9-c, d), from temperate

oceanic climate (Fig. 9- c-e) to temperate sub-continental (Fig. 9-a, f), or even subtropic climate (Fig. 9-b), all filed details

were indicated clearly in our maps. Fragmentation of land in some European countries, especially in Eastern and Central

Europe after land reform in 1989 (Hartvigsen, 2013, 2014), such as Estonia (Fig.7f) (Jürgenson and Rasva, 2020; Looga et al.,

315 2018). Although under different climate, terrain, landscapes and over very larger region, the algorithm proposed in our study

consistently shows a good classification accuracy across 33 countries. Thus, the rapeseed maps based on S1/2 data can

effectively identify the fields in detail with high spatial resolutions and clear field boundaries. More rapeseed classification

details can be found in Fig. S12 and Fig. S18.

Furthermore, our results showed a consistent distributions between our rapeseed maps and the existing products at the pixel
320   level (Fig. S13). The yellow grids (71%~80%) mean they are simultaneously identified as rapeseed areas both by our method
and ACI/CDL/CROME, while red grids for disagreement. The difference in accuracy might be caused by the number of high-
quality images available in different regions (Dong et al., 2016). Despite the various ground conditions, methods, images, and
spatial resolutions among the products, the comparison results further verify the accuracy of our rapeseed map (Gong et al.,
2020; Singha et al., 2019).
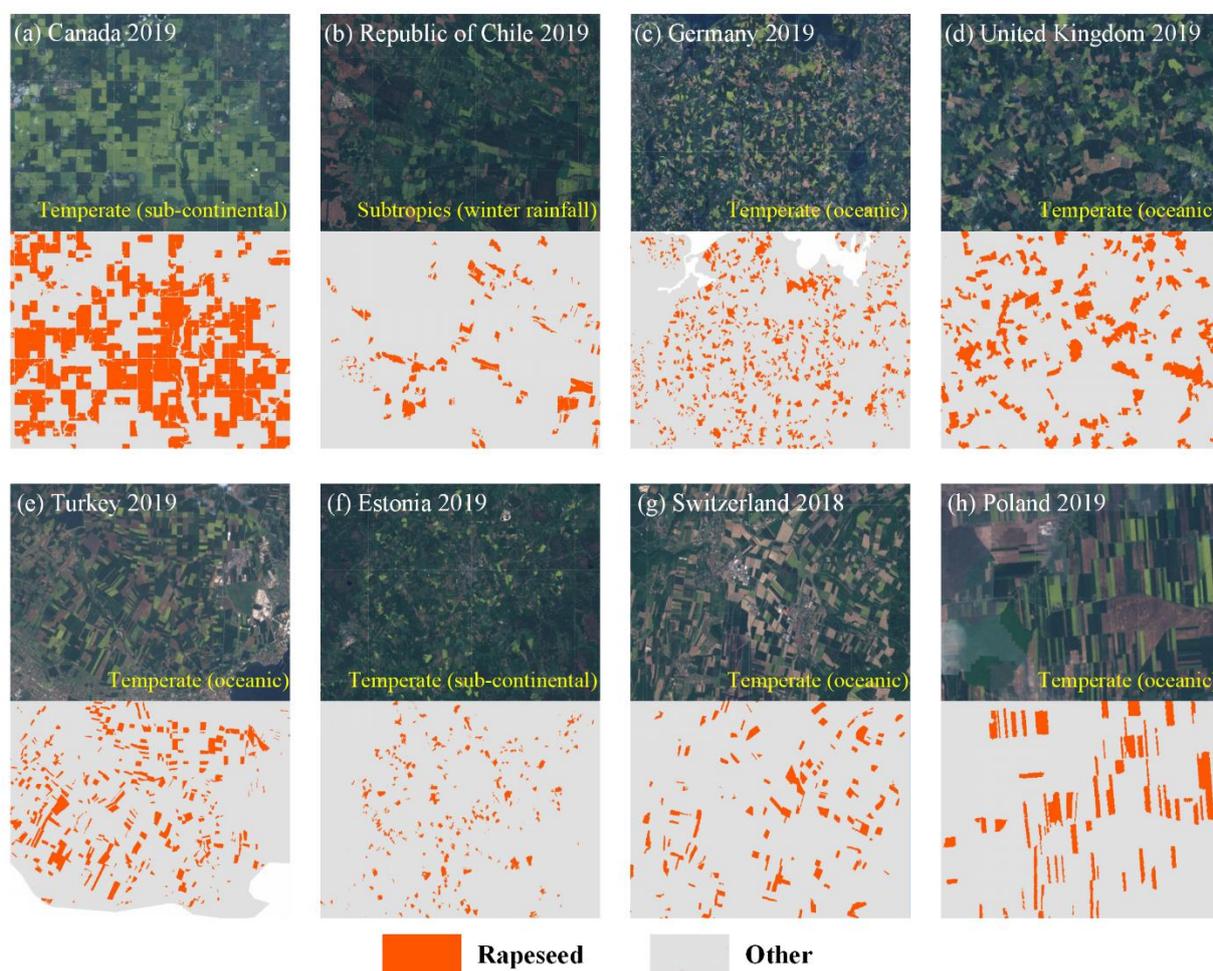
325

Figure 7. Spatially-explicit details of rapeseed maps in eight countries with diverse crop structures in different years (the yellow
words show the climatic zones). The upper layers were RGB composite images using the red (b4), green(b3), and blue (b2)
bands from Sentinel-2 with good-quality observations during the flowering period of rapeseed (image source: Copernicus
Sentinel-2 data).   The climate zone data is from the Food Insecurity, Poverty and Environment Global GIS Database (FGGD).

3.3 Spatial patterns of rapeseed planting areas

Canada shows the largest rapeseed planting area (Fig. 8, Fig. S14), with the total area of 118,489.73 km^2 in 2018, higher than those in Europe (106,814.67 km^2). France and Germany are two leading rapeseed growing countries in Europe, accounting for around 66.3% European rapeseed areas together with other three countries (United Kingdom, Poland, and Ukraine). The country-wide rapeseed areas in all 33 countries were further normalized to show clearly the spatial patterns (Fig. S14). The spatial patterns of three years (2017~2019) are consistent at the national level. Moreover, we also plotted the geographic characteristics of rapeseed areas along latitude and longitude by three regions (Fig. 8). Rapeseed in Europe is widely planted in the countries with a latitude of 45~56°N and longitude of -2°~4°, 9°~19°, and 22°~27°, with exception of the steep mountainous areas and the cold northern areas (Fig. 8a) (van Duren et al., 2015). In North America, the areas with latitude of 44~44.5°N, 51~55°N, 56~57°N and longitude of -118°~-117°, -114°~-98°are densely distributed by rapeseed (Fig. 8b).
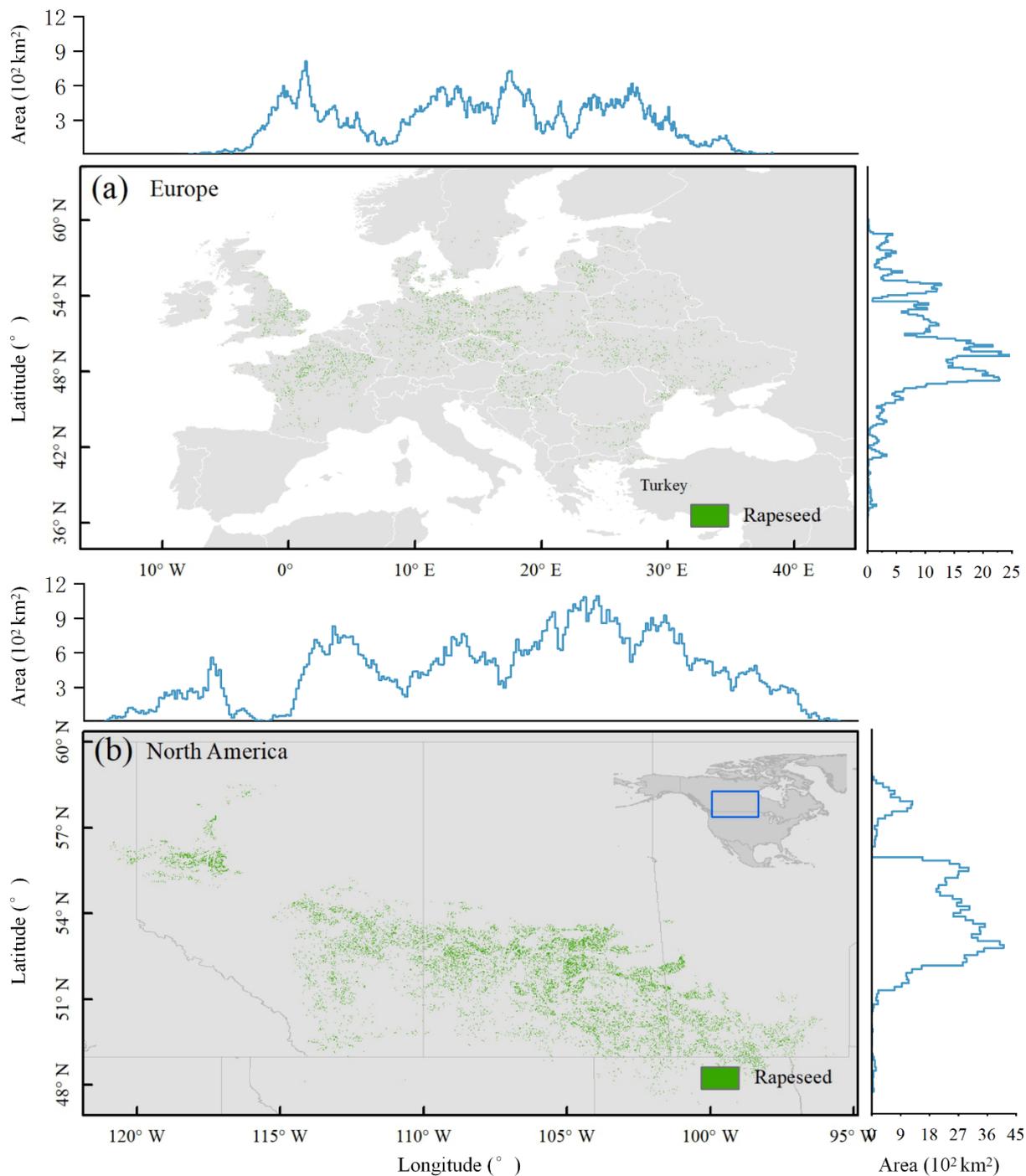
Figure 8. Spatial distribution of rapeseed areas at 10m-resolution along latitude and longitude gradients in 2018, (a) Europe and Turkey, (b) Canada and America.

4 Discussion

4.1 Investigating the rapeseed rotation systems

345 We obtained three-year rapeseed maps at a 10m spatial resolution, and with a higher accurancy which was validated by annual national statitisc books, open accessed public products and random sampling points at 0.2°x 0.2°grids. These rapeseed maps, with good quality for three consecutive years, provide a new opportunity to investigate rapeseed rotation systems (Liu et al., 2018a). Crop rotation information is considered as an important factor for yield, soil degradation, and greenhouse gas emissions (Harker et al., 2015; Liu et al., 2018a; Ren et al., 2015; Rudiyanto et al., 2019; Zhou et al., 2015). Thus, we selected 25

350 representative areas (Fig. S15) to analyze the rapeseed rotation patterns according to the three criterions: 1) high-quality images available during the annual rapeseed flowering period from 2017 to 2019; 2) high rapeseed classification accuracy; 3) rapeseed is the main crop type and a large area is planted by rapeseed every year. The rapeseed rotation was calculated by the frequency in each rapeseed pixel (Fig. S16-17).

We classfied the rapeseed rotation break into three types: ≥2 years, 1 year, 0 year (Fig. 9 and Fig. S16-17. We found most

355 countries show the rotation break ≥2 years (the highest ratios of green parts) (Fig. 9), especially for European countries (Fig. 9-b). The rotation break ≥2 years in Canada mounts to 70%, followed by 30% with 1-year break (Fig. 9-a). The histogram futher confirmed that 20 locations have identified as the rotation break ≥2 years, with their rates of planting areas higher than 90% (Fig. 9-d). Many previous studies have found that a two- or three-year rotation break will significantly reduce the number of spores, especially rhizomes and blacklegs, suggesting rotation system is an important step in controlling diseases (Gill, 2018;

360 Harker et al., 2015; Ren et al., 2015; Zhou et al., 2015). Moreover, rapeseed rotation will also benefit yield, insects, moisture, fertility, and reducing weeds (Bernard et al., 2012; Harker et al., 2015; Pardo et al., 2015; Peng et al., 2015; Ren et al., 2015). Thus, more efforts should be input to produce longer time-series rapeseed maps, and obtain detailed rotation information in the future.
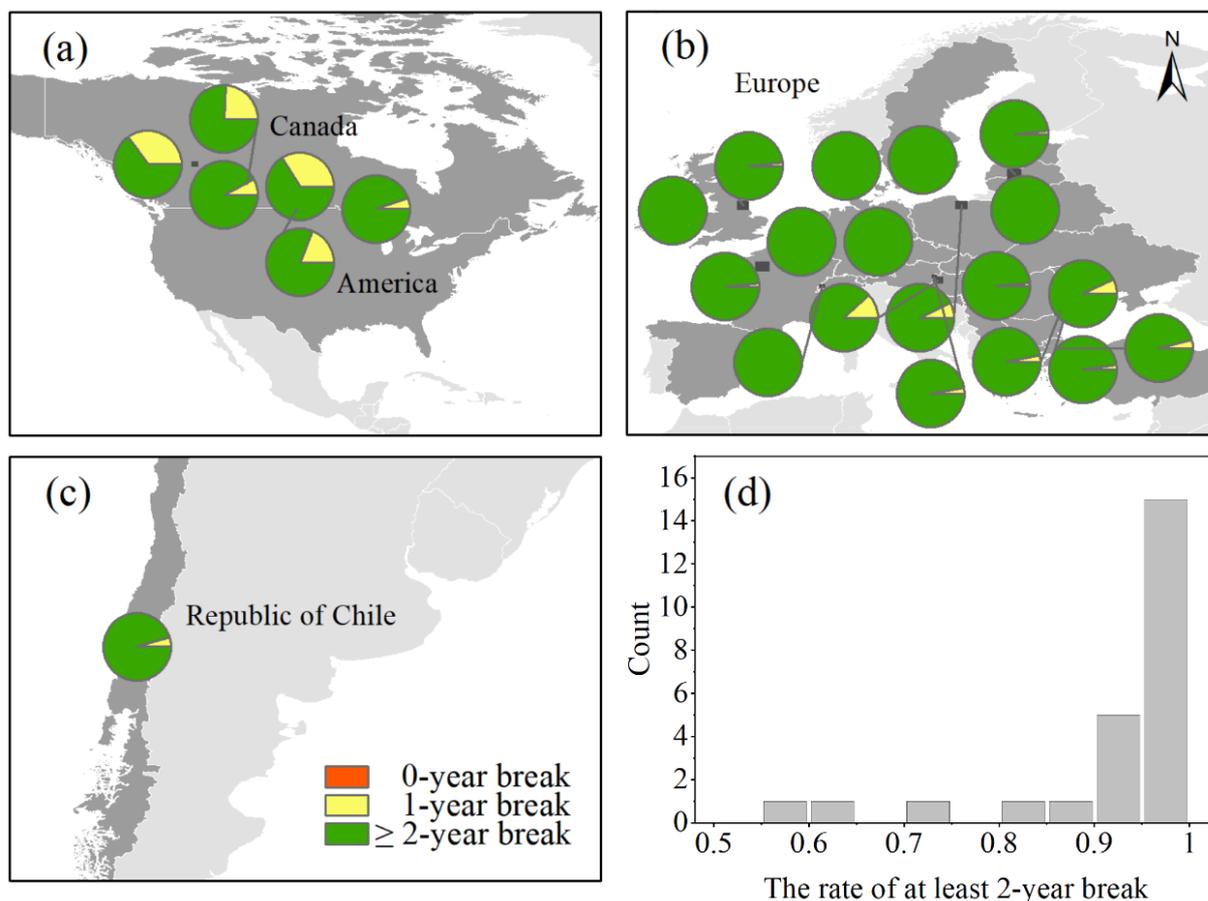
365   Figure 9 (a-c) The proportion of three types of rapeseed rotations to the total area planted by rapeseed. The scope of each area
selected can be found in the red rectangle in Fig. S15. (d) The histogram of green parts (≥ 2-year break) in Fig. 9 a-c.

4.2 Uncertainty analysis

Generating annual high-resolution maps of a specific crop over a larger region is a big challenge (Gong et al., 2020; Liu et al.,
2018b, 2020a). Pixel-and phenological-based algorithms, multisource remote sensing data, and the GEE are useful to map
370   rapeseed with high-resolution and over larger areas. Besides, the algorithm does not need training sample data and reduces
disturbance from agronomy differences by combining images of multiple dates. However, the uncertainty are from the follows:
1) cropland layer. We used the GFSAD30 datasets to identify croplands. However, GFSAD30 has its limitations such as
classification error (Phalke et al., 2020). *2) the number of satellite images available*. Although our annual rapeseed maps are
consistent with FAO statistics, and show higher accuracy comparing with existing products, the maps are limited by the good-
375   quality observations during the critical growth stages. For example, Fig. 10a shows that the error in the area of France in 2017,
and error could be attributed to the lack of clear S2 images during rapeseed flowering period (Fig. 10b). Rapeseed flowering
period is generally characterized by higher NDYI, red band, and green band reflectance, thus missing the peak will fail in

identifying rapeseed pixels (Fig. 10c). *3) thresholds for different indicators*. The threshold is the key for mapping crop
(Ashourloo et al., 2019; Dong et al., 2016; Liu et al., 2020a; Wang et al., 2020a; Zhang et al., 2015). Although the reference

380   thresholds for three regions are given in this study, it should be cautious when applying them into other regions. 4) *the
complexity of ground environment.* For example, landscape types might impact the accuracy of rapeseed map (Wang et al.,
2020a).
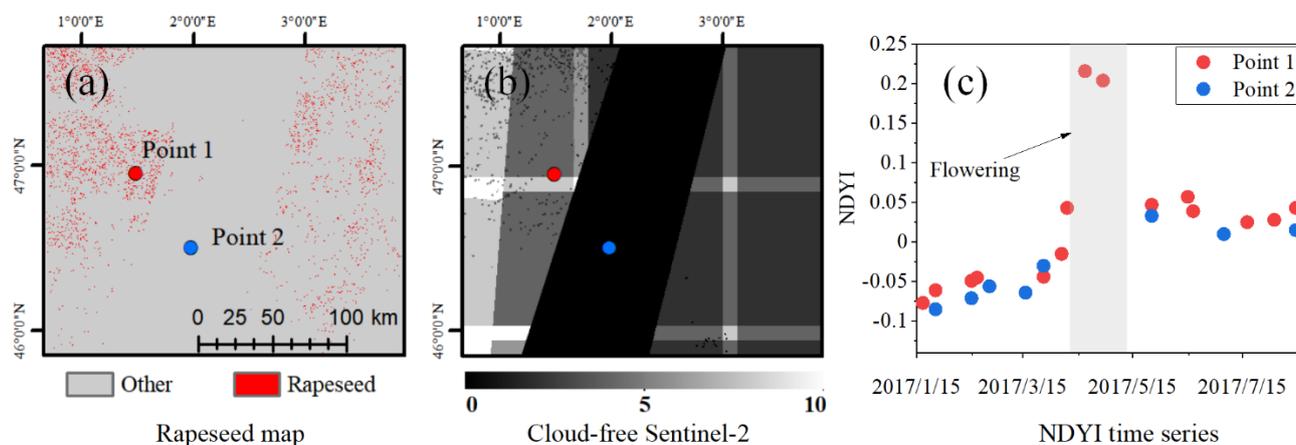
Figure 10. (a) Rapeseed map with an error in France in 2017 (2°6'35.368"E, 46°44'5.953"N). (b) Availability of time series

385   Sentinel-2 images during rapeseed flowering phases. (c) Comparison of the time series of different rapeseed parcels indicating
how the peak NDYI is missed.

4.3 Implications and improvements

Despite the above limitations, the new phenology-based method proposed by us has the potential to extend to other regions by
revising the phenology metrics. Recently, the Harmonized Landsat and Sentinel-2 database improve the spatial resolution and

390   revisit cycle of images (Claverie et al., 2018; Shang and Zhu, 2019). Similar or even higher rapeseed classification accuracy
can be expected. Furthermore, remote sensing data fusion algorithms have been continuously developed (e.g., STARFM and
ESTARFM) (Zhu et al., 2010). Finnally, various deep learning models have been explored for classifying crops and lowering
errors (Hu et al., 2019; Zhong et al., 2019). Integrating phenological metrics and deep learning models might further improve
rapeseed mapping accuracy. Thus, such rapeseed products will objectively track the dynamics of rapeseed planting areas as

395   well as agricultural management in the future.

5 Data availability

The rapeseed map produced is accessible at Mendeley Data (http://dx.doi.org/10.17632/ydf3m7pd4j.3) (Han et al., 2021). The
rapeseed maps with 10 m resolution are provided in this study. The dataset includes a set of GeoTIFF images in the ESPG:
4326 spatial reference system. The values 1 and 0 represent rapeseed and non-rapeseed, respectively. We encourage users to

400   independently verify the rapeseed map. In addition, S 1/2 images, CDL, ACI, and SRTM are available on GEE (https://developers.google.com/earth-engine/datasets/). For more detailed information about the data collected in this work, please see Table 1.

6 Conclusions

Large-scale and high-resolution rapeseed maps are the basis for crop growth monitoring and production prediction. We
405   designed a new method for mapping rapeseed based on the spectral and polarization feature and multi-source data. The new algorithm have produced three annual rapeseed maps (2017~2019) at 10m spatial resolution in 33 countries. Three different verification methods indicate that our products have relatively higher accuracy. Our approach reduces disturbances from different planting time and bad-quality observations in some degree. The 10m rapeseed maps do provide more spatial details of rapeseed. Also, we have found that rapeseed crop rotation is 2 years or more in almost all countries. The rapeseed mapping
410   method proposed in this study could be applied into other regions and other crops. The derived rapeseed data product is useful for many purposes including crop growth monitoring and production, rotation systems planning.

Author contributions

ZZ and JH designed the research. JH and LY collected datasets. JH implemented the research and wrote the paper. ZZ, JC,
415   LZ, JZ, and ZL revised the paper.

Declaration of competing interest

The authors declare that they have no known competing financial interests or personal relationships that could have appeared to influence the work reported in this paper.

420

Acknowledgement

This work was supported by the National Key Research and Development Program of China (project nos. 019YFA0607401).

References

d'Andrimont, R., Taymans, M., Lemoine, G., Ceglar, A., Yordanov, M. and van der Velde, M.: Detecting flowering phenology
425   in oil seed rape parcels with Sentinel-1 and -2 time series, Remote Sensing of Environment, 239, 111660, https://doi.org/10.1016/j.rse.2020.111660, 2020.

Arata, L., Fabrizi, E. and Sckokai, P.: A worldwide analysis of trend in crop yields and yield variability: Evidence from FAO data, Economic Modelling, 90, 190–208, https://doi.org/10.1016/j.econmod.2020.05.006, 2020.

Arino, O., Bicheron, P., Achard, F., Latham, J., Witt, R. and Weber, J.-L.: The most detailed portrait of Earth, Eur. Space
430   Agency, 136, 25–31, 2008.

Ashourloo, D., Shahrabi, H. S., Azadbakht, M., Aghighi, H., Nematollahi, H., Alimohammadi, A. and Matkan, A. A.: Automatic canola mapping using time series of sentinel 2 images, ISPRS Journal of Photogrammetry and Remote Sensing, 156, 63–76, https://doi.org/10.1016/j.isprsjprs.2019.08.007, 2019.

Bargiel, D.: A new method for crop classification combining time series of radar images and crop phenology information, Remote Sensing of Environment, 198, 369–383, https://doi.org/10.1016/j.rse.2017.06.022, 2017.

Bartholomé, E. and Belward, A. S.: GLC2000: a new approach to global land cover mapping from Earth observation data, International Journal of Remote Sensing, 26(9), 1959–1977, https://doi.org/10.1080/01431160412331291297, 2005.

Bernard, E., Larkin, R. P., Tavantzis, S., Erich, M. S., Alyokhin, A., Sewell, G., Lannan, A. and Gross, S. D.: Compost, rapeseed rotation, and biocontrol agents significantly impact soil microbial communities in organic and conventional potato production systems, Applied Soil Ecology, 52, 29–41, https://doi.org/10.1016/j.apsoil.2011.10.002, 2012.

Boryan, C., Yang, Z., Mueller, R. and Craig, M.: Monitoring US agriculture: the US Department of Agriculture, National Agricultural Statistics Service, Cropland Data Layer Program, Geocarto International, 26(5), 341–358, https://doi.org/10.1080/10106049.2011.562309, 2011.

Carré, P. and Pouzet, A.: Rapeseed market, worldwide and in Europe, OCL, 21(1), D102, https://doi.org/10.1051/ocl/2013054, 2014.

Chen, B., Jin, Y. and Brown, P.: An enhanced bloom index for quantifying floral phenology using multi-scale remote sensing observations, ISPRS Journal of Photogrammetry and Remote Sensing, 156, 108–120, https://doi.org/10.1016/j.isprsjprs.2019.08.006, 2019.

Chen, J., Jönsson, Per., Tamura, M., Gu, Z., Matsushita, B. and Eklundh, L.: A simple method for reconstructing a high-quality NDVI time-series data set based on the Savitzky–Golay filter, Remote Sensing of Environment, 91(3–4), 332–344, https://doi.org/10.1016/j.rse.2004.03.014, 2004.

Claverie, M., Ju, J., Masek, J. G., Dungan, J. L., Vermote, E. F., Roger, J.-C., Skakun, S. V. and Justice, C.: The Harmonized Landsat and Sentinel-2 surface reflectance data set, Remote Sensing of Environment, 219, 145–161, https://doi.org/10.1016/j.rse.2018.09.002, 2018.

Dong, J., Xiao, X., Menarguez, M. A., Zhang, G., Qin, Y., Thau, D., Biradar, C. and Moore, B.: Mapping paddy rice planting area in northeastern Asia with Landsat 8 images, phenology-based algorithm and Google Earth Engine, Remote Sensing of Environment, 185, 142–154, https://doi.org/10.1016/j.rse.2016.02.016, 2016.

Drusch, M., Del Bello, U., Carlier, S., Colin, O., Fernandez, V., Gascon, F., Hoersch, B., Isola, C., Laberinti, P., Martimort, P., Meygret, A., Spoto, F., Sy, O., Marchese, F. and Bargellini, P.: Sentinel-2: ESA's Optical High-Resolution Mission for GMES Operational Services, Remote Sensing of Environment, 120, 25–36, https://doi.org/10.1016/j.rse.2011.11.026, 2012.

van Duren, I., Voinov, A., Arodudu, O. and Firrisa, M. T.: Where to produce rapeseed biodiesel and why? Mapping European rapeseed energy efficiency, Renewable Energy, 74, 49–59, https://doi.org/10.1016/j.renene.2014.07.016, 2015.

ESA, 2015a. Sentinel-2 products specification document.
465   https://sentinel.esa.int/documents/247904/349490/S2_MSI_Product_Specification.pdf Accessed date: 24 April 2019.

ESA, 2015b. Data Product Quality Reports. https://sentinels.copernicus.eu/documents/247904/3902831/Sentinel-2_L1C_Data_Quality_Report/adfff903-a337-4fc1-9439-558456bad0b1?version=1.1

Fang, S., Tang, W., Peng, Y., Gong, Y., Dai, C., Chai, R. and Liu, K.: Remote Estimation of Vegetation Fraction and Flower Fraction in Oilseed Rape with Unmanned Aerial Vehicle Data, Remote Sensing, 8(5), 416,
470   https://doi.org/10.3390/rs8050416, 2016.

Farr, T. G., Rosen, P. A., Caro, E., Crippen, R., Duren, R., Hensley, S., Kobrick, M., Paller, M., Rodriguez, E. and Roth, L.: The shuttle radar topography mission, Reviews of geophysics, 45(2), 2007.

Firrisa, M. T., van Duren, I. and Voinov, A.: Energy efficiency for rapeseed biodiesel production in different farming systems, Energy Efficiency, 7(1), 79–95, https://doi.org/10.1007/s12053-013-9201-2, 2014.

475   Fisette, T., Rollin, P., Aly, Z., Campbell, L., Daneshfar, B., Filyer, P., Smith, A., Davidson, A., Shang, J. and Jarvis, I.: AAFC annual crop inventory, in 2013 Second International Conference on Agro-Geoinformatics (Agro-Geoinformatics), pp. 270–274, IEEE, Fairfax, VA, USA, https://doi.org/10.1109/Argo-Geoinformatics.2013.6621920, , 2013.

Frantz, D., Haß, E., Uhl, A., Stoffels, J. and Hill, J.: Improvement of the Fmask algorithm for Sentinel-2 images: Separating clouds from bright surfaces based on parallax effects, Remote Sensing of Environment, 215, 471–481,
480   https://doi.org/10.1016/j.rse.2018.04.046, 2018.

Fuglie, K. O.: Total factor productivity in the global agricultural economy: Evidence from FAO data, The shifting patterns of agricultural production and productivity worldwide, 63–95, 2010.

Gill, K. S.: Crop rotations compared with continuous canola and wheat for crop production and fertilizer use over 6 yr, edited by C. Willenborg, Can. J. Plant Sci., 98(5), 1139–1149, https://doi.org/10.1139/cjps-2017-0292, 2018.

485   Gong, P., Wang, J., Yu, L., Zhao, Y., Zhao, Y., Liang, L., Niu, Z., Huang, X., Fu, H., Liu, S., Li, C., Li, X., Fu, W., Liu, C., Xu, Y., Wang, X., Cheng, Q., Hu, L., Yao, W., Zhang, H., Zhu, P., Zhao, Z., Zhang, H., Zheng, Y., Ji, L., Zhang, Y., Chen, H., Yan, A., Guo, J., Yu, L., Wang, L., Liu, X., Shi, T., Zhu, M., Chen, Y., Yang, G., Tang, P., Xu, B., Giri, C., Clinton, N., Zhu, Z., Chen, J. and Chen, J.: Finer resolution observation and monitoring of global land cover: first mapping results with Landsat TM and ETM+ data, International Journal of Remote Sensing, 34(7), 2607–2654,
490   https://doi.org/10.1080/01431161.2012.748992, 2013.

Gong, P., Li, X., Wang, J., Bai, Y., Chen, B., Hu, T., Liu, X., Xu, B., Yang, J., Zhang, W. and Zhou, Y.: Annual maps of global artificial impervious area (GAIA) between 1985 and 2018, Remote Sensing of Environment, 236, 111510, https://doi.org/10.1016/j.rse.2019.111510, 2020.

Gorelick, N., Hancher, M., Dixon, M., Ilyushchenko, S., Thau, D. and Moore, R.: Google Earth Engine: Planetary-scale
495   geospatial analysis for everyone, Remote Sensing of Environment, 202, 18–27, https://doi.org/10.1016/j.rse.2017.06.031, 2017.

Griffiths, P., Nendel, C. and Hostert, P.: Intra-annual reflectance composites from Sentinel-2 and Landsat for national-scale crop and land cover mapping, Remote Sensing of Environment, 220, 135–151, https://doi.org/10.1016/j.rse.2018.10.031, 2019.

500   Han, J., Zhang, Z. and Cao, J.: Developing a New Method to Identify Flowering Dynamics of Rapeseed Using Landsat 8 and Sentinel-1/2, Remote Sensing, 13(1), 105, https://doi.org/10.3390/rs13010105, 2020.

Han, J., Zhang, Z., Luo, Y., Cao, J., Zhang, L., Zhang, J., Li, Z.: Data for: Developing a phenology- and pixel-based algorithm for mapping rapeseed at 10m spatial resolution using multi-source data, Mendeley Data, V3, doi: 10.17632/ydf3m7pd4j.3, 2021.

505   Harker, K. N., O'Donovan, J. T., Turkington, T. K., Blackshaw, R. E., Lupwayi, N. Z., Smith, E. G., Johnson, E. N., Gan, Y., Kutcher, H. R., Dosdall, L. M. and Peng, G.: Canola rotation frequency impacts canola yield and associated pest species, Can. J. Plant Sci., 95(1), 9–20, https://doi.org/10.4141/cjps-2014-289, 2015.

Hartvigsen, M.: Land reform in Central and Eastern Europe after 1989 and its outcome in the form of farm structures and land fragmentation, Citeseer., 2013.

510   Hartvigsen, M.: Land reform and land fragmentation in Central and Eastern Europe, Land Use Policy, 36, 330–341, https://doi.org/10.1016/j.landusepol.2013.08.016, 2014.

Hassan, M. Hj. and Kalam, Md. A.: An Overview of Biofuel as a Renewable Energy Source: Development and Challenges, Procedia Engineering, 56, 39–53, https://doi.org/10.1016/j.proeng.2013.03.087, 2013.

Hirayama, H., Sharma, R. C., Tomita, M. and Hara, K.: Evaluating multiple classifier system for the reduction of salt-and-
515   pepper noise in the classification of very-high-resolution satellite images, International Journal of Remote Sensing, 40(7), 2542–2557, https://doi.org/10.1080/01431161.2018.1528400, 2019.

Höök, M. and Tang, X.: Depletion of fossil fuels and anthropogenic climate change—A review, Energy Policy, 52, 797–809, https://doi.org/10.1016/j.enpol.2012.10.046, 2013.

Hu, W., Patel, J. H., Robert, Z.-A., Novosad, P., Asher, S., Tang, Z., Burke, M., Lobell, D. and Ermon, S.: Mapping Missing
520   Population in Rural India: A Deep Learning Approach with Satellite Imagery, in Proceedings of the 2019 AAAI/ACM Conference on AI, Ethics, and Society, pp. 353–359, ACM, Honolulu HI USA, https://doi.org/10.1145/3306618.3314263, 2019.

Jarasiunas, G.: Assessment of the agricultural land under steep slope in Lithuania, j. cent. eur. agric., 17(1), 176–187, https://doi.org/10.5513/JCEA01/17.1.1688, 2016.

525   Jürgenson, E. and Rasva, M.: The Changing Structure and Concentration of Agricultural Land Holdings in Estonia and Possible Threat for Rural Areas, Land, 9(2), 41, https://doi.org/10.3390/land9020041, 2020.

Kaspar, F., Zimmermann, K. and Polte-Rudolf, C.: An overview of the phenological observation network and the phenological database of Germany's national meteorological service (Deutscher Wetterdienst), Adv. Sci. Res., 11(1), 93–99, https://doi.org/10.5194/asr-11-93-2014, 2015.

530   Liu, J., Zhu, W., Atzberger, C., Zhao, A., Pan, Y. and Huang, X.: A Phenology-Based Method to Map Cropping Patterns under
        a Wheat-Maize Rotation Using Remotely Sensed Time-Series Data, Remote Sensing, 10(8), 1203,
        https://doi.org/10.3390/rs10081203, 2018a.

Liu, X., Hu, G., Chen, Y., Li, X., Xu, X., Li, S., Pei, F. and Wang, S.: High-resolution multi-temporal mapping of global urban
        land using Landsat images based on the Google Earth Engine Platform, Remote Sensing of Environment, 209, 227–239,
535   https://doi.org/10.1016/j.rse.2018.02.055, 2018b.

Liu, X., Huang, Y., Xu, X., Li, X., Li, X., Ciais, P., Lin, P., Gong, K., Ziegler, A. D., Chen, A., Gong, P., Chen, J., Hu, G.,
        Chen, Y., Wang, S., Wu, Q., Huang, K., Estes, L. and Zeng, Z.: High-spatiotemporal-resolution mapping of global urban
        change from 1985 to 2015, Nat Sustain, 3(7), 564–570, https://doi.org/10.1038/s41893-020-0521-x, 2020a.

Liu, Y., Xu, B., Zhi, W., Hu, C., Dong, Y., Jin, S., Lu, Y., Chen, T., Xu, W., Liu, Y., Zhao, B. and Lu, W.: Space eye on flying
540   aircraft: From Sentinel-2 MSI parallax to hybrid computing, Remote Sensing of Environment, 246, 111867,
        https://doi.org/10.1016/j.rse.2020.111867, 2020b.

Looga, J., Jürgenson, E., Sikk, K., Matveev, E. and Maasikamäe, S.: Land fragmentation and other determinants of agricultural
        farm productivity: The case of Estonia, Land Use Policy, 79, 285–292, https://doi.org/10.1016/j.landusepol.2018.08.021,
        2018.

545   Lowder, S. K., Skoet, J. and Raney, T.: The Number, Size, and Distribution of Farms, Smallholder Farms, and Family Farms
        Worldwide, World Development, 87, 16–29, https://doi.org/10.1016/j.worlddev.2015.10.041, 2016.

Luo, Y., Zhang, Z., Chen, Y., Li, Z. and Tao, F.: ChinaCropPhen1km: a high-resolution crop phenological dataset for three
        staple crops in China during 2000–2015 based on leaf area index (LAI) products, Earth Syst. Sci. Data, 12(1), 197–214,
        https://doi.org/10.5194/essd-12-197-2020, 2020.

550   Malça, J. and Freire, F.: Energy and Environmental Benefits of Rapeseed Oil Replacing Diesel, International Journal of Green
        Energy, 6(3), 287–301, https://doi.org/10.1080/15435070902886551, 2009.

Malenovský, Z., Rott, H., Cihlar, J., Schaepman, M. E., García-Santos, G., Fernandes, R. and Berger, M.: Sentinels for science:
        Potential of Sentinel-1, -2, and -3 missions for scientific observations of ocean, cryosphere, and land, Remote Sensing of
        Environment, 120, 91–101, https://doi.org/10.1016/j.rse.2011.09.026, 2012.

555   McNairn, H., Champagne, C., Shang, J., Holmstrom, D. and Reichert, G.: Integration of optical and Synthetic Aperture Radar
        (SAR) imagery for delivering operational annual crop inventories, ISPRS Journal of Photogrammetry and Remote
        Sensing, 64(5), 434–449, https://doi.org/10.1016/j.isprsjprs.2008.07.006, 2009.

McNairn, H., Jiao, X., Pacheco, A., Sinha, A., Tan, W. and Li, Y.: Estimating canola phenology using synthetic aperture radar,
        Remote Sensing of Environment, 219, 196–205, https://doi.org/10.1016/j.rse.2018.10.012, 2018.

560   Mercier, A., Betbeder, J., Baudry, J., Le Roux, V., Spicher, F., Lacoux, J., Roger, D. and Hubert-Moy, L.: Evaluation of
        Sentinel-1 & 2 time series for predicting wheat and rapeseed phenological stages, ISPRS Journal of Photogrammetry and
        Remote Sensing, 163, 231–256, https://doi.org/10.1016/j.isprsjprs.2020.03.009, 2020.

Pan, Z., Huang, J. and Wang, F.: Multi range spectral feature fitting for hyperspectral imagery in extracting oilseed rape planting area, International Journal of Applied Earth Observation and Geoinformation, 25, 21–29, https://doi.org/10.1016/j.jag.2013.03.002, 2013.

Pardo, N., Sánchez, M. L., Pérez, I. A. and García, M. A.: Energy balance and partitioning over a rotating rapeseed crop, Agricultural Water Management, 161, 31–40, https://doi.org/10.1016/j.agwat.2015.07.015, 2015.

Peel, M. C., Finlayson, B. L. and McMahon, T. A.: Updated world map of the Köppen-Geiger climate classification, Hydrol. Earth Syst. Sci., 11(5), 1633–1644, https://doi.org/10.5194/hess-11-1633-2007, 2007.

Pekel, J.-F., Cottam, A., Gorelick, N. and Belward, A. S.: High-resolution mapping of global surface water and its long-term changes, Nature, 540(7633), 418–422, https://doi.org/10.1038/nature20584, 2016.

Peng, G., Pageau, D., Strelkov, S. E., Gossen, B. D., Hwang, S.-F. and Lahlali, R.: A >2-year crop rotation reduces resting spores of Plasmodiophora brassicae in soil and the impact of clubroot on canola, European Journal of Agronomy, 70, 78–84, https://doi.org/10.1016/j.eja.2015.07.007, 2015.

Phalke, A. R., Özdoğan, M., Thenkabail, P. S., Erickson, T., Gorelick, N., Yadav, K. and Congalton, R. G.: Mapping croplands of Europe, Middle East, Russia, and Central Asia using Landsat, Random Forest, and Google Earth Engine, ISPRS Journal of Photogrammetry and Remote Sensing, 167, 104–122, https://doi.org/10.1016/j.isprsjprs.2020.06.022, 2020.

Preidl, S., Lange, M. and Doktor, D.: Introducing APiC for regionalised land cover mapping on the national scale using Sentinel-2A imagery, Remote Sensing of Environment, 240, 111673, https://doi.org/10.1016/j.rse.2020.111673, 2020.

Ren, T., Li, H., Lu, J., Bu, R., Li, X., Cong, R. and Lu, M.: Crop rotation-dependent yield responses to fertilization in winter oilseed rape (Brassica napus L.), The Crop Journal, 3(5), 396–404, https://doi.org/10.1016/j.cj.2015.04.007, 2015.

Rondanini, D. P., Gomez, N. V., Agosti, M. B. and Miralles, D. J.: Global trends of rapeseed grain yield stability and rapeseed-to-wheat yield ratio in the last four decades, European Journal of Agronomy, 37(1), 56–65, https://doi.org/10.1016/j.eja.2011.10.005, 2012.

Rondanini, D. P., del Pilar Vilariño, M., Roberts, M. E., Polosa, M. A. and Botto, J. F.: Physiological responses of spring rapeseed (Brassica napus) to red/far-red ratios and irradiance during pre- and post-flowering stages, Physiol Plantarum, 152(4), 784–794, https://doi.org/10.1111/ppl.12227, 2014.

Rudiyanto, Minasny, Shah, Soh, Arif, and Setiawan: Automated Near-Real-Time Mapping and Monitoring of Rice Extent, Cropping Patterns, and Growth Stages in Southeast Asia Using Sentinel-1 Time Series on a Google Earth Engine Platform, Remote Sensing, 11(14), 1666, https://doi.org/10.3390/rs11141666, 2019.

Salmon, J. M., Friedl, M. A., Frolking, S., Wisser, D. and Douglas, E. M.: Global rain-fed, irrigated, and paddy croplands: A new high resolution map derived from remote sensing, crop inventories and climate data, International Journal of Applied Earth Observation and Geoinformation, 38, 321–334, https://doi.org/10.1016/j.jag.2015.01.014, 2015.

Shafiee, S. and Topal, E.: When will fossil fuel reserves be diminished?, Energy Policy, 37(1), 181–189, https://doi.org/10.1016/j.enpol.2008.08.016, 2009.

Shang, R. and Zhu, Z.: Harmonizing Landsat 8 and Sentinel-2: A time-series-based reflectance adjustment approach, Remote Sensing of Environment, 235, 111439, https://doi.org/10.1016/j.rse.2019.111439, 2019.

She, B., Huang, J., Guo, R., Wang, H. and Wang, J.: Assessing winter oilseed rape freeze injury based on Chinese HJ remote sensing data, J. Zhejiang Univ. Sci. B, 16(2), 131–144, https://doi.org/10.1631/jzus.B1400150, 2015.

600 Singha, M., Dong, J., Zhang, G. and Xiao, X.: High resolution paddy rice maps in cloud-prone Bangladesh and Northeast India using Sentinel-1 data, Sci Data, 6(1), 26, https://doi.org/10.1038/s41597-019-0036-3, 2019.

Sulik, J. J. and Long, D. S.: Spectral indices for yellow canola flowers, International Journal of Remote Sensing, 36(10), 2751–2765, https://doi.org/10.1080/01431161.2015.1047994, 2015.

Sulik, J. J. and Long, D. S.: Spectral considerations for modeling yield of canola, Remote Sensing of Environment, 184, 161–
605 174, https://doi.org/10.1016/j.rse.2016.06.016, 2016.

Tao, J., Wu, W., Liu, W. and Xu, M.: Exploring the Spatio-Temporal Dynamics of Winter Rape on the Middle Reaches of Yangtze River Valley Using Time-Series MODIS Data, Sustainability, 12(2), 466, https://doi.org/10.3390/su12020466, 2020.

Teluguntla, P., Thenkabail, P. S., Oliphant, A., Xiong, J., Gumma, M. K., Congalton, R. G., Yadav, K. and Huete, A.: A 30-
610 m landsat-derived cropland extent product of Australia and China using random forest machine learning algorithm on Google Earth Engine cloud computing platform, ISPRS Journal of Photogrammetry and Remote Sensing, 144, 325–340, https://doi.org/10.1016/j.isprsjprs.2018.07.017, 2018.

Tian, H., Meng, M., Wu, M. and Niu, Z.: Mapping spring canola and spring wheat using Radarsat-2 and Landsat-8 images with Google Earth Engine, Curr. Sci, 116(2), 291–298, 2019.

615 Torres, R., Snoeij, P., Geudtner, D., Bibby, D., Davidson, M., Attema, E., Potin, P., Rommen, B., Floury, N., Brown, M., Traver, I. N., Deghaye, P., Duesmann, B., Rosich, B., Miranda, N., Bruno, C., L'Abbate, M., Croci, R., Pietropaolo, A., Huchler, M. and Rostan, F.: GMES Sentinel-1 mission, Remote Sensing of Environment, 120, 9–24, https://doi.org/10.1016/j.rse.2011.05.028, 2012.

Van Tricht, K., Gobin, A., Gilliams, S. and Piccard, I.: Synergistic Use of Radar Sentinel-1 and Optical Sentinel-2 Imagery
620 for Crop Mapping: A Case Study for Belgium, Remote Sensing, 10(10), 1642, https://doi.org/10.3390/rs10101642, 2018.

Veloso, A., Mermoz, S., Bouvet, A., Le Toan, T., Planells, M., Dejoux, J.-F. and Ceschia, E.: Understanding the temporal behavior of crops using Sentinel-1 and Sentinel-2-like data for agricultural applications, Remote Sensing of Environment, 199, 415–426, https://doi.org/10.1016/j.rse.2017.07.015, 2017.

Wang, D., Fang, S., Yang, Z., Wang, L., Tang, W., Li, Y. and Tong, C.: A Regional Mapping Method for Oilseed Rape Based
625 on HSV Transformation and Spectral Features, IJGI, 7(6), 224, https://doi.org/10.3390/ijgi7060224, 2018.

Wang, J., Xiao, X., Liu, L., Wu, X., Qin, Y., Steiner, J. L. and Dong, J.: Mapping sugarcane plantation dynamics in Guangxi, China, by time series Sentinel-1, Sentinel-2 and Landsat images, Remote Sensing of Environment, 247, 111951, https://doi.org/10.1016/j.rse.2020.111951, 2020a.

Wang, X., Xiao, X., Zou, Z., Dong, J., Qin, Y., Doughty, R. B., Menarguez, M. A., Chen, B., Wang, J., Ye, H., Ma, J., Zhong, Q., Zhao, B. and Li, B.: Gainers and losers of surface and terrestrial water resources in China during 1989–2016, Nat Commun, 11(1), 3471, https://doi.org/10.1038/s41467-020-17103-w, 2020b.

Wang, X., Xiao, X., Zou, Z., Hou, L., Qin, Y., Dong, J., Doughty, R. B., Chen, B., Zhang, X., Chen, Y., Ma, J., Zhao, B. and Li, B.: Mapping coastal wetlands of China using time series Landsat images in 2018 and Google Earth Engine, ISPRS Journal of Photogrammetry and Remote Sensing, 163, 312–326, https://doi.org/10.1016/j.isprsjprs.2020.03.014, 2020c.

Xiao, X., Boles, S., Frolking, S., Li, C., Babu, J. Y., Salas, W. and Moore, B.: Mapping paddy rice agriculture in South and Southeast Asia using multi-temporal MODIS images, Remote Sensing of Environment, 100(1), 95–113, https://doi.org/10.1016/j.rse.2005.10.004, 2006.

Xiong, J., Thenkabail, P., Tilton, J., Gumma, M., Teluguntla, P., Oliphant, A., Congalton, R., Yadav, K. and Gorelick, N.: Nominal 30-m Cropland Extent Map of Continental Africa by Integrating Pixel-Based and Object-Based Algorithms Using Sentinel-2 and Landsat-8 Data on Google Earth Engine, Remote Sensing, 9(10), 1065, https://doi.org/10.3390/rs9101065, 2017.

Zhang, G., Xiao, X., Dong, J., Kou, W., Jin, C., Qin, Y., Zhou, Y., Wang, J., Menarguez, M. A. and Biradar, C.: Mapping paddy rice planting areas through time series analysis of MODIS land surface temperature and vegetation index data, ISPRS Journal of Photogrammetry and Remote Sensing, 106, 157–171, https://doi.org/10.1016/j.isprsjprs.2015.05.011, 2015.

Zhang, G., Xiao, X., Dong, J., Xin, F., Zhang, Y., Qin, Y., Doughty, R. B. and Moore, B.: Fingerprint of rice paddies in spatial–temporal dynamics of atmospheric methane concentration in monsoon Asia, Nat Commun, 11(1), 554, https://doi.org/10.1038/s41467-019-14155-5, 2020.

Zhang, Y., Chipanshi, A., Daneshfar, B., Koiter, L., Champagne, C., Davidson, A., Reichert, G. and Bédard, F.: Effect of using crop specific masks on earth observation based crop yield forecasting across Canada, Remote Sensing Applications: Society and Environment, 13, 121–137, https://doi.org/10.1016/j.rsase.2018.10.002, 2019.

Zhao, F., Xia, L., Kylling, A., Li, R. Q., Shang, H. and Xu, M.: Detection flying aircraft from Landsat 8 OLI data, ISPRS Journal of Photogrammetry and Remote Sensing, 141, 176–184, https://doi.org/10.1016/j.isprsjprs.2018.05.001, 2018.

Zhong, L., Gong, P. and Biging, G. S.: Efficient corn and soybean mapping with temporal extendability: A multi-year experiment using Landsat imagery, Remote Sensing of Environment, 140, 1–13, https://doi.org/10.1016/j.rse.2013.08.023, 2014.

Zhong, L., Hu, L., Yu, L., Gong, P. and Biging, G. S.: Automated mapping of soybean and corn using phenology, ISPRS Journal of Photogrammetry and Remote Sensing, 119, 151–164, https://doi.org/10.1016/j.isprsjprs.2016.05.014, 2016.

Zhong, L., Hu, L. and Zhou, H.: Deep learning based multi-temporal crop classification, Remote Sensing of Environment, 221, 430–443, https://doi.org/10.1016/j.rse.2018.11.032, 2019.

Zhou, M., Zhu, B., Brüggemann, N., Wang, X., Zheng, X. and Butterbach-Bahl, K.: Nitrous oxide and methane emissions from a subtropical rice–rapeseed rotation system in China: A 3-year field case study, Agriculture, Ecosystems & Environment, 212, 297–309, https://doi.org/10.1016/j.agee.2015.07.010, 2015.

Zhu, X., Chen, J., Gao, F., Chen, X. and Masek, J. G.: An enhanced spatial and temporal adaptive reflectance fusion model
665   for complex heterogeneous regions, Remote Sensing of Environment, 114(11), 2610–2623, https://doi.org/10.1016/j.rse.2010.05.032, 2010.

Zhu, Z., Wang, S. and Woodcock, C. E.: Improvement and expansion of the Fmask algorithm: cloud, cloud shadow, and snow detection for Landsats 4–7, 8, and Sentinel 2 images, Remote Sensing of Environment, 159, 269–277, https://doi.org/10.1016/j.rse.2014.12.014, 2015.

670 Zou, Z., Xiao, X., Dong, J., Qin, Y., Doughty, R. B., Menarguez, M. A., Zhang, G. and Wang, J.: Divergent trends of open-surface water body area in the contiguous United States from 1984 to 2016, Proc Natl Acad Sci USA, 115(15), 3810–3815, https://doi.org/10.1073/pnas.1719275115, 2018.